

Water megamaser emission in hard X-ray selected AGN

F. Panessa¹, P. Castangia², A. Malizia³, L. Bassani³, A. Tarchi², A. Bazzano¹, and P. Ubertini¹

¹ Istituto di Astrofisica e Planetologia Spaziali di Roma (IAPS-INAF), Via del Fosso del Cavaliere 100, 00133 Roma, Italy
e-mail: francesca.panessa@inaf.it

² Osservatorio Astronomico di Cagliari (OAC-INAF), Via della Scienza 5, 09047 Selargius (CA), Italy

³ Osservatorio di Astrofisica e Scienza dello Spazio di Bologna (OAS-INAF), Via P. Gobetti 101, 40129 Bologna, Italy

Received ; accepted

ABSTRACT

Context. Water megamaser emission at 22 GHz has proven to be a powerful tool for astrophysical studies of AGN allowing an accurate determination of the central black hole mass and of the accretion disc geometry and dynamics. However, after searches among thousands of galaxies, only ~ 200 of them have shown such spectroscopic features, most of them of uncertain classification. In addition, the physical and geometrical conditions under which maser activates are still unknown.

Aims. In this work we aim at characterizing the occurrence of water maser emission in an unbiased sample of AGN, investigating the relation with the X-ray properties and the possible favorable geometry needed to detect water maser.

Methods. We have searched for 22 GHz maser emission in a hard X-ray selected sample of AGN, taken from the INTEGRAL/IBIS survey above 20 keV. Of the 380 sources in the sample, only half have water maser data. We have also considered a sub-sample of 87 sources, volume limited, for which we obtained new Green Bank Telescope and Effelsberg observations (for 35 sources), detecting one new maser and increasing its radio coverage to 75%.

Results. The detection rate of water maser emission in the total sample is $15\pm3\%$, this fraction raises up to $19\pm5\%$ for the complete sub-sample, especially if considering type 2 ($22\pm5\%$ and $31\pm10\%$ for the total and complete samples respectively) and Compton thick AGN ($56\pm18\%$ and $50\pm35\%$ for the total and complete samples respectively). No correlation is found between water maser and X-ray luminosity. We have noted that all type of masers (disc/jet) are associated to hard X-ray selected AGN.

Conclusions. These results demonstrate that the hard X-ray selection may significantly enhance the maser detection efficiency over comparably large optical/infrared surveys. A possible decline of the detection fraction with increasing luminosity might suggest that an extreme luminous nuclear environment does not favour maser emission. The large fraction of CT AGN with water maser emission could be explained in terms of geometrical effects, being the maser medium the very edge-on portion of the obscuring medium.

Key words. galaxies: active — galaxies: Seyfert — masers — X-rays: galaxies — gamma-rays: galaxies — surveys

1. Introduction

One of the most common maser emission line is from the water rotational transition levels 6_{16} and 5_{23} , emitting at 22 GHz in the radio domain. Extra-galactic water masers trace warm ($T_{\text{kin}} > 300$ K) and dense ($10^7 \text{ cm}^{-3} < n(\text{H}_2) < 10^{11} \text{ cm}^{-3}$) gas (Elitzur 1992; Neufeld et al. 1994). Water maser sources with an isotropic luminosity below $10 L_{\odot}$ are defined as kilo-masers, while at higher luminosity they are defined as mega-masers, the latter are generally associated to the activity of Active Galactic Nuclei (AGN), while kilo-masers are more commonly related to star-formation in the host galaxy¹

The activity of water maser emission in AGN has been associated to three main different phenomena (see e. g. Lo 2005; Tarchi 2012). A typical triple-peak system of lines is associated to an accretion disc emission (one systemic, one blueshifted and one redshifted), whose geometry and rotation velocities can be traced by Very Long Baseline Interferometry (VLBI, e. g. Miyoshi et al. 1995; Greenhill et al. 2003a). On the other hand, the interaction between the radio jet and the molecular clouds or the overlap along the line of sight between the molecular cloud and radio continuum emission from the jet could produce water maser emission in the form of a single broad redshifted (or

blueshifted) line (e. g. Gallimore et al. 2001, 1996, Henkel et al. 2005). Jet velocity and density were estimated via reverberation mapping analysis (Peck et al. 2003). Finally, in the case of the Circinus galaxy, the water maser emission has shown two different dynamic components via VLBI mapping: one associated with a warped disc while the other with a wide angle nuclear outflow (Greenhill et al. 2003a). Outflowing maser components have been detected also in NGC 3079 (Kondratko et al. 2005).

So far, more than 4000 galaxies have been searched for water maser emission and detections have been obtained in about ~ 160 of them (180 if starbursts galaxies are also included, Megamaser Cosmology Project, MCP²), the majority being radio-quiet AGN in the local Universe ($z \leq 0.05$), classified as Seyfert 2 or Low-ionization nuclear emission-line regions (LINERs). The overall detection rate in large maser surveys is rather low (e.g., Braatz et al. 1997; Greenhill et al. 2003; Van den Bosch et al. 2016) and is around 3% among sources observed within the MCP, that mainly targets galaxies selected from large optical surveys, such as SDSS, 6dF and 2MRS (Braatz et al. 2015; see also Greenhill et al. 2003b; Zhu et al. 2011). Hagiwara et al. (2002; 2003), by selecting their targets based on the ratio of radio continuum to IR (60μ and 100μ) flux densities from IRAS galaxies, obtained a slightly higher detection rate of 8%. That

¹ This distinction should, however, be used with caution, see Tarchi et al. (2011a; their Sect. 4.2) and this work (Sect.3).

² <https://safe.nrao.edu/wiki/bin/view/Main/MegamaserCosmologyProject>

the far-infrared selection favours maser detection was later confirmed by Henkel et al. (2005) who found a detection rate of 22% among a sample of northern galaxies having IRAS point source flux density at $100\ \mu$ greater than 50 mJy. More recently, Kuo et al. (2018) found that galaxies with water maser detection tend to be associated with strong infrared emission as observed by the WISE telescope, thus offering a way to boost the detection rate to 6-15%. It has also been suggested radio emission as a suitable indicator for water maser emission (Zhang et al. 2012; 2017), indeed maser galaxies tend to have higher radio luminosities by a factor of 2–3 than the non-masing ones (Liu et al. 2017).

Finally, the fraction of water maser detection has been found to be around 26% in a sample of Seyfert galaxies located within 20 Mpc, suggesting that an observational bias in terms of distance is also likely to occur (Panessa & Giroletti 2013).

Selecting high luminosity objects might improve maser detection efficiency (Zhu et al. 2011). However, the largest fraction of nuclear water masers seem to be associated with type 2 Seyfert galaxies and high level of X-ray obscuration (Greenhill et al. 2008), in particular to Compton-thick (CT) AGN³ (Greenhill et al. 2003b; Castangia et al. 2019). This is in line with the predictions of Unified Models for AGN (Antonucci & Miller 1985), in which at larger scales an obscuring torus aligned with the accretion disc is responsible for the observed obscuration and for the optical classification of the AGN (see Padovani et al. 2017 for a review). Interestingly, the fraction of CT obscuration increases in disc masers (Greenhill et al. 2008), as confirmed by X-ray studies of known disc masers (Castangia et al. 2013; Masini et al. 2016). In order to be detected, maser discs should be observed nearly edge-on to the observer line of sight, suggesting a connection between the X-ray obscuring material and the maser disc. Indeed, masers could trace molecular material associated with the torus or the outer regions of the accretion disc. All the different proposed geometries (e.g., Elitzur & Shlosman 2006; Tilak et al. 2008; Masini et al. 2016) take into account that long path lengths are needed to produce maser amplification, therefore the observer line of sight has to be close to an edge-on orientation. In this respect, warped discs, as indeed observed in the prototype NGC 4258 (Herrnstein et al. 1997), increase the chances of intercepting the line of sight. As a matter of fact the disc has to be warped to be directly illuminated by the X-ray radiation coming from the central engine, as envisaged by the theory of maser production (Neufeld et al. 1994). More recently, Darling (2017) discussed the interesting possibility to detect also some water maser sources associated with inclined accretion discs (more than 10 degrees from edge-on) orbiting massive black holes via the lensing or deflection of in-going systemic maser features.

Even if higher X-ray luminosity and/or higher column density objects more likely host masers, so far there is no large sample of AGN with X-ray data available for target selection nor a similar type of study have been performed on statistically meaningful basis. This work aims at filling this gap and at providing some useful means to improve maser detection efficiency by pre-selecting targets from hard X-ray surveys, which so far are the less biased in terms of AGN intrinsic absorption.

Throughout this paper we assume a flat Λ CDM cosmology with $(\Omega_M, \Omega_\Lambda) = (0.3, 0.7)$ and a Hubble constant of $70\ \text{km s}^{-1}\ \text{Mpc}^{-1}$ (Jarosik et al. 2011).

2. Sample definition

In this work we concentrate on a sample of active galaxies selected in hard X-rays (or soft gamma-ray band, defined above 20 keV). This waveband provides a very efficient way to find nearby AGN (both un-absorbed and absorbed), since it is transparent to obscured regions/objects, i.e. those that could be missed at other frequencies such as optical, UV, and even X-rays below 10 keV. Since 2002, the hard X-ray sky is being surveyed by INTEGRAL/IBIS (Ubertini et al. 2003) and subsequently by Swift/BAT (Gehrels et al. 2004) at energies greater than ~ 20 keV; up to now various all sky catalogues have been released, based on the data collected by these two satellites (see for example Bird et al. 2016; Baumgartner et al. 2013 and Oh et al. 2018). These catalogues contain large fractions of active galaxies, i.e. $\sim 40\%$ among INTEGRAL/IBIS and up to 70% among Swift/BAT sources. Together these two samples provide the most extensive list of hard X-ray selected active galaxies known to date.

For the purpose of this work, we use the large sample of AGN extracted from INTEGRAL/IBIS data and only for comparison purposes we consulted two samples extracted from Swift/BAT surveys (the 9 month and 70 month ones).

For INTEGRAL, we consider the sample of 272 AGN discussed by Malizia et al. (2012), added with 108 sources that have been discovered or identified with active galaxies afterwards (Malizia et al. 2016). This set of 380 hard X-ray selected AGN represents our reference catalogue and will be used as the main input for this work. The main advantage of this sample is that it is fully characterized in terms of optical class, redshift and X-ray properties, including information on the X and hard X-ray fluxes and X-ray column density. Unfortunately, due to the INTEGRAL observing strategy, this sample is not complete nor uniform and so to overcome this limitation we consider a subset of AGN (all included in the sample of 380 objects) which represent instead a complete sample. This sample, which is fully discussed in Malizia et al. (2009), is made of 87 galaxies⁴ detected in the 20–40 keV band and listed in the 3rd IBIS survey (Bird et al. 2007). To investigate for maser emission in the entire sample of 380 AGN, we consulted the catalogues maintained on the Web site of the MCP which is the largest and most comprehensive catalogue of all galaxies surveyed for water maser emission at 22 GHz (Reid et al. 2009; Braatz et al. 2010); the catalogue has been updated on a regular basis to include all of the new observations and associated findings. To integrate the MCP data, as well as to cover as much as possible our sample, we also searched the literature for report of water maser observations/detections. Finally, 35 galaxies belonging to the complete sample have been observed, for the first time, in search for 22 GHz water maser emission using the Effelsberg and the Green Bank Telescope and a new maser has been discovered (Sect. 3). Table 1A lists all 380 INTEGRAL/IBIS AGN (see Appendix A for a detailed description).

In Fig. 1 we plot the hard X-ray luminosity as a function of redshift (in logarithmic scale) for the total sample (left panel) and the complete sample (right panel), dividing the AGN between those not observed at 22 GHz (green dots), those observed (blue stars) and the ones detected (red open polygons). It is clear from this figure that objects at high redshift and high hard X-ray luminosity are almost not covered by maser observations. Furthermore, we have compared the distributions in redshift and luminosities between the total and complete samples in order to check if they belong to the same parent population (null hy-

³ Compton-thick AGN are defined as sources with X-ray obscuration $N_H > 10^{24}\ \text{cm}^{-2}$, the inverse of the Thomson cross section.

⁴ We note that one source, IGR J03184-0014, is not considered here as it was never detected again in subsequent INTEGRAL surveys.

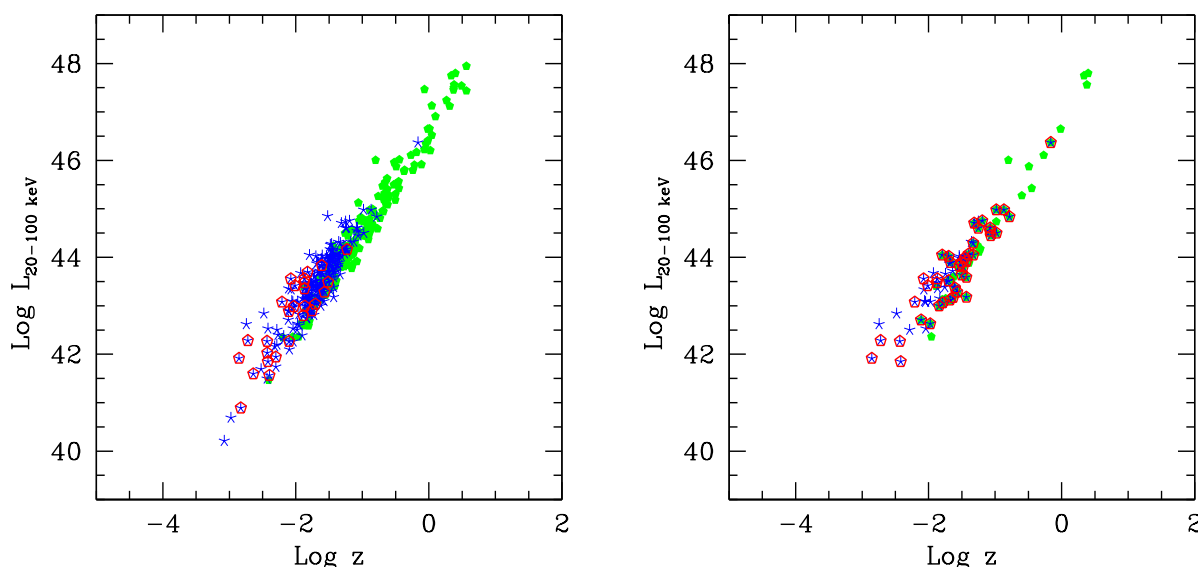


Fig. 1: Hard X-ray luminosity (20–100 keV) versus the logarithm of the redshift, the green dots are those sources not observed at 22 GHz, the blue stars are those observed and the red open polygons are the ones detected. Left panel: total sample of 380 AGN. Right panel: complete sub-sample of 87 AGN.

pothesis). A Kolmogorov–Smirnov (KS) test results in p -values of 0.10 (z) and 0.59 ($L_{20-100\text{keV}}$), therefore the null hypothesis cannot be rejected at the 1% level. This suggests that the two samples could be considered statistically equivalent, i.e., likely affected by similar biases. We have performed the same test considering only observed sources in the two samples. The KS test results in p -values of 0.75 (z) and 0.41 ($L_{20-100\text{keV}}$), again the null hypothesis cannot be rejected at the 1% level. We can conclude that both the total and the complete samples of hard X-rays selected AGN with water maser observations are representative of the local Universe and thus constitute an ideal set where to study water maser occurrence in nearby super-massive black holes.

3. Observations, data reduction and results

3.1. GBT observations

We observed the $6_{16}-5_{23}$ transition of ortho- H_2O (rest frequency 22.23508 GHz) toward 28 galaxies of the complete INTEGRAL sample with the Green Bank Telescope (GBT), between March 2010 and January 2011 (projects AGBT10A-042 and AGBT10C-012). We used the 18–22 GHz dual beam receiver in nod mode, keeping one of the two beams alternatively on-source during integration. The GBT spectrometer was configured with two 200 MHz IFs offset by 180 MHz, for a total coverage of 380 MHz (corresponding to 5100 km s^{-1} at 22 GHz). The first spectral window was centered at the frequency corresponding to the recessional velocity of each galaxy and the second was offset to the red. This setup yielded a channel spacing of 24 kHz ($\sim 0.3 \text{ km s}^{-1}$ at 22 GHz) per spectral window. We reduced and analysed the data with `GBTIDL`⁵. Flux calibration was performed using standard routines and applying the default zenith opacity

and gain curve. The estimated uncertainty of the absolute flux calibration is $\sim 20\%$ (for details see the guide for calibrating GBT spectral line data using `GBTIDL`⁶).

3.2. Effelsberg observations

On April 15 and 16, 2011, we used the Effelsberg 100-m telescope to search for 22 GHz water maser emission in seven galaxies of the complete INTEGRAL sample (3C 111, IC 4329A, IGR J16482, 2E 1739, IGR J17513, IGR J21247, and BL LAC). We employed the 1.3 cm primary focus (PFK) receiver (17.9–26.2 GHz) with an FFTS spectrometer encompassing 100 MHz and 16384 channels. This setup yielded a channel spacing of 6.1 kHz, corresponding to 0.08 km s^{-1} at 22.2 GHz. We observed in a position switching mode, with the off-position offset by 15 arcminutes in right ascension. Signals from individual on- and off-source positions were integrated for 120 s each. The data were reduced using the `GILDAS` software package (e.g. Guilleaume & Lucas 2000). To convert the measured signal from counts to antenna temperature we utilized the tabulated values of the noise diode in K. We then applied the normalized gain curve and multiplied for the standard value of the sensitivity⁷. The uncertainty of this flux calibration was derived applying the same procedure to continuum pointing scans of NGC 7027 and is estimated to be $\sim 30\%$.

⁶ https://www.gb.nrao.edu/GBT/DA/gbtidl/gbtidl_calibration.pdf

⁷ Calibration information for the 1.3 cm PFK receiver are reported in the Effelsberg Wiki page <https://eff100mwiki.mpi-fr-bonn.mpg.de/doku.php>.

⁵ <http://gbtidl.nrao.edu>

3.3. Results

During our survey, a new water maser was detected with the GBT in the Narrow Line Seyfert 1 (NLSy1) galaxy IGR J16385-2057, on March 28, 2010. This discovery, and hence the line profile and the characteristics of the water maser emission, has been anticipated in a previous paper by our team, which was focused on water maser emission in NLSy1 galaxies (Tarchi et al. 2011b). Here, in Table 1A, we report the isotropic line luminosity. In Table 1A we also list the 1σ rms and the upper limit on $L_{\text{H}_2\text{O}}$ for the remaining 33 targets, with the exception of 3C 273. Indeed, due to the strong radio continuum emission of the blazar's jet ($S_{22}=27\text{--}43$ Jy, e.g. Gear et al. 1994), the GBT spectral baseline is affected by strong ripples that prevented us to estimate a reliable rms for this source and to assess the presence (or absence) of an emission line, as a consequence 3C 273 is labeled as 'not observed' in Table 1A.

Although we could not reach the full coverage of the complete sample at 22 GHz, we were able to bring the number of sources with water maser observations from the initial 31 with data in the literature to 65 (34 from our own survey), increasing the coverage from 36% to 75%.

Within the sample of 34 objects observed for the first time, maser detection rate is rather low ($1/34$ or $<6\%$), however this is likely due to the optical classification of observed sources: the majority of the objects (26) belong to the type 1 classification whereas only 8 sources are of type 2. The only one detected belongs to the class of NLSy1, that indeed seems to have a large probability to host maser emission (Tarchi et al. 2011b). In this respect, the fraction of detected maser within these newly-observed AGN is consistent with the average fraction of detected maser among type 1 objects (see next Sect.). We have also checked for further biases introduced by the lack of full radio observation coverage of the complete sample, other than the known bias against high redshift and luminosity. We have compared the distribution of X-ray absorption and position in the sky of the observed and non observed sources. The test did not reveal significant differences between the two sub-samples in terms of absorption (KS p -value=0.09) nor position in the sky (KS p -value=0.23).

4. Maser fraction at high energies

Out of 380 objects in the total sample, 193 have been observed at 22 GHz, only $51\pm4\%$ of the sample; concerning instead the complete sample, 65 out of 87 objects were observed at this frequency, providing a coverage of almost 75%.

Considering the total set of INTEGRAL AGN reported in Table 1A, we found that out of 193 galaxies observed at 22 GHz, 29 have been reported as maser sources; this represents a detection rate of $15\pm3\%$ ⁸. To take into account unobserved sources and thus provide a range of values for the entire sample, we can take two extreme approaches and assume that, if pointed, all not yet observed INTEGRAL AGN will turn out to be undetected at 22 GHz (lower range) or alternatively that all will be detected (upper range). Under these conditions we find that the detection rate for the whole sample ranges from 8 to 57%, a rather large range which nevertheless tells us that the detection rate is in the worst case higher than generally obtained using large samples of optically-selected galaxies (Sect. 1). Out of 29 objects with

maser detection, 6 have a 22 GHz luminosity below $10 L_{\odot}$ (i.e., Mkn 3, NGC 4051, NGC 4151, Mkn 766, Cen A and NGC 6300) and therefore qualify to be kilo-maser objects. However, some of these sources have been imaged at high resolution and their maser emission found to be located within the nuclear region of the host galaxies. Therefore, given that all our sources are hard X-ray emitters and can be confidently associated with accreting supermassive black hole, we confirm that kilo-maser emission may not only be associated to star formation but also to AGN activity, as already suggested by Tarchi et al. (2011a).

Considering instead the complete sample of INTEGRAL sources highlighted in Table 1A, we have 65 AGN observed at 22 GHz of which 12 detected and only 22 not observed: in this case the detection rate is $19\pm5\%$ and the range of possible values is between 14 and 39%.

Given the preference for water maser emitters to be found in type 2 AGN, we also restricted our analysis to only Seyfert 2 (including intermediate types 1.8-1.9) which are present either in the total or in the complete INTEGRAL samples. In this case we find that the sample coverage was 68% (103 AGN observed, 23 detected and 60 not observed) and 88% (29 AGN observed, 9 detected and 5 not observed) for the total and complete sample respectively: we estimate therefore a detection rate of $22\pm5\%$ (range values from 14 to 51%) and $31\pm10\%$ (range values from 27 to 41%) for each of these two samples.

These fractions are even more remarkable if compared to those of Seyfert 1 (including also in this case intermediate types 1.2-1.5): 74 objects have water maser observations among type 1 AGN, but only two (i.e., NGC 4151 and NGC 3783) have been detected implying a detection fraction of around 3%, i.e. similar to what found within the MCP (see also König et al. 2012). Interestingly NLSy1, which are also broad line AGN but with peculiar characteristics at multi-frequencies with respect to standard broad line AGN (see e.g., Panessa et al. 2011), show a detection rate comparable to those of Seyfert 2. In our sample, there are 9 NLSy1 with 22 GHz measurements and 3 water maser detections (NGC 4051, Mkn 766 and IGR J16385-2057) implying rates close to 30%. This confirms previous results obtained by Tarchi et al. (2011b) in a dedicated study of this type of AGN in which the authors suggest an outflow origin for water maser emission. Mathur (2000) proposed that NLSy1 sources can be young AGN residing in rejuvenated galaxies; alternatively, their peculiarities can be explained in terms of an orientation effect, ascribed to their broad-line region being observed pole-on (Decarli et al. 2008). How these two interpretations can be linked to the maser phenomenon in these peculiar objects is still unclear but confirmation of high detection rates in NLSy1 indicates that the issue requires more in depth studies.

To consolidate our overall results we have also compared the above rates with those obtained from the 70 months (Baumgartner et al. 2013) and 9 months (Tueller et al. 2008) Swift/BAT samples. These two samples have been selected to be almost comparable in size with the INTEGRAL total and complete sub-samples.

The 70 month BAT survey provides the list of all objects detected by the instrument during the first 6.8 years of the Swift mission and covers 90% of the sky at a sensitivity level of 1.3×10^{-11} ergs $\text{s}^{-1} \text{cm}^{-2}$ in the 14-195 keV band. The sample contains a large fraction of unclassified sources which may turn out to be AGN, after proper follow up work; thus our search for maser detection provides only an indication of the level of maser oc-

⁸ Errors on the fractions have been calculated as $\sqrt{N_M}/N_O$, where N_M is the number of detected maser sources and N_O is the number of observed sources.

Table 1: Summary of the detection fractions for different samples/sub-samples.

Sample (Number of AGN observed at 22GHz)	DF (Detection Fraction in %)	DF (Detection Fraction in %)range
INTEGRAL Total (285)	15.0±2.8	7.6-57.0
INTEGRAL Complete (65)	18.5±5.3	13.8-39.0
INTEGRAL Sey1.8-2 Total (103)	22.0±4.7	13.5-51.0
INTEGRAL Sey1.8-2 Complete (29)	31±10	27-41
INTEGRAL Sey1-1.5 Total (74)	2.7±1.9	1.4-51.0
INTEGRAL NLSy1 Total (9)	33±19	20-60
Swift/BAT 70M (285)	12.6±2.1	-
Swift/BAT 9M (114)	14.9±3.6	11-37
Swift/BAT 9M Sey2 (51)	25.5±7.0	20-41
DS optical (89)	23.6±5.1	-
DS optical Sey2(71)	26.8±6.1	-

currence in this large BAT sample⁹. As already done for the INTEGRAL sample, we searched the available archives such as the MCP and the literature to look for reports of water maser observations as well as detections for all 822 AGN reported in the BAT survey. All together we found that out of this sample only 285 objects (therefore only 35% of the sample) have been observed at 22 GHz and 36 objects have been detected¹⁰. The detection fraction is therefore around 13±2%, in perfect agreement with our INTEGRAL results.

The Swift/BAT 9 month catalogue contains only 154 sources (all of which are identified and optically classified as AGN) and covers 74% of the sky (only the sky above ±15 degrees in latitude have been considered to avoid galactic object contamination) at a flux threshold of 5×10^{-11} ergs s⁻¹ cm⁻² in the 14-195 keV band. In this catalogue, 114 objects have been observed at 22 GHz and 17 detected (listed in Table 2A). Only 40 AGN have no observational coverage at the waveband of interest here. The detection rate is 15±4%. Applying the same exercise as done for the INTEGRAL samples (i.e., assuming all unobserved sources to be either detected or not at 22 GHz) we estimate a possible range of values between 11 and 37%. If we restrict to only type 2 AGN, we have 65 objects in this sample of which 51 have been observed, with 13 objects displaying maser emission; this provides a detection rate close to 26±7%; in this case the possible range of values is estimated to vary from 20 to 41%, again in full agreement with the estimates obtained from the INTEGRAL samples.

Finally, we have compared our results, in particularly those obtained for type 2 Seyferts, with the optical data set of AGN discussed by Diamond-Stanic et al. (2009). These authors have compiled a complete sample of 89 Seyfert galaxies, made of 18 type 1 (1-1.5) and 71 type 2 (1.8-2) AGN all within a distance of 200 Mpc. The entire sample has been covered by water maser observations and is therefore a reference catalogue for this type of studies. There are 21 maser (listed in Table 3A) and 68 non maser sources in this sample providing a detection rate of 24±5%. If we restrict the estimate to only Seyfert 2 galaxies,

the detection rate increases only slightly to 27%, again in full agreement with the estimate provided in this work. The highest detection rate found in this sample seems to be in contrast with estimates obtained using other optically selected sample of AGN (for example in their work, Zhu et al. (2011) quote a detection rate for Seyfert 2 close to 8%), but this maybe due to the fact that the Diamond-Stanic et al. (2009) sample is biased in favour of close-by AGN, mostly of type 2, similarly to the sample investigated in Panessa & Giroletti (2013).

The detection fractions for all samples considered in this work are summarized in Table 1, where it is clear that hard X-ray catalogues provide a significant boost of maser detection fraction with respect to large optical surveys (e.g. Zhu et al. 2011; Braatz et al. 2018), reaching values of at least 15-25%. These values are also higher than those obtained by specifically tuning AGN selection in the infrared band using different criteria and combining them together as recently proposed by Kuo et al. (2018). Furthermore, the hard X-ray selection, beside providing a catalogue of galaxies with a high probability of maser detection, it also gives a set of sources with clear evidence of AGN activity and therefore negligible or null contamination from star forming objects.

5. Improving detection probability

In Fig. 2, we plot the water maser detection rate in our total sample (blue stars) and in the complete sub-sample (magenta polygons) as a function of redshift (left panel), X-ray nuclear absorption (middle panel) and 20-100 keV hard X-ray luminosity (right panel). For the distribution of water maser fraction as a function of redshift and column density, objects have been grouped in order to have roughly the same number of observed sources per bin. For the distribution in luminosity instead this was more difficult to achieve while still maintaining a reasonable number of bins, however the uncertainty related to this choice is reflected in the error associated to each bin.

It is evident that water maser detection decreases as a function of redshift, from around 40-60% at low redshifts down to a few percent at higher distances (above $z=0.015$), in agreement with the distance bias discussed in Sect. 2 and 3. On the contrary the detection fraction increases for higher X-ray column densities going from a few percent up to 25-40% at a threshold of 10^{23} cm⁻² and reaching 56±18% above the Compton thick regime in the case of the total sample (50±35 for the complete sample), again confirming that the water maser detection is favoured among heavily absorbed AGN. Also the hard X-ray luminosity seems to play a role, although in this cases the error bars are larger and the scarce observations of high luminous

⁹ To search for water maser emission in this set of hard X-ray selected AGN, we were helped by 3 high school students during a stage performed at OAS/INAF in Bologna in the summer of 2016.

¹⁰ Most of these detections overlap with the INTEGRAL ones; the extra sources are NGC 235A, UGC 3157, VII Zw 073, NGC 3393, CGCG 164-019, MKN 78, UGC 5101 and M 82 considering that IGR J16385-2057 and NGC 6926 were only detected by INTEGRAL. We note that in the case of M 82 the emission above 10 keV is dominated by a few ultra-luminous X-ray sources (ULXs) with a minor contribution from lower luminosity X-ray binaries (Vulic et al. 2018) and therefore cannot be attributed to AGN activity.

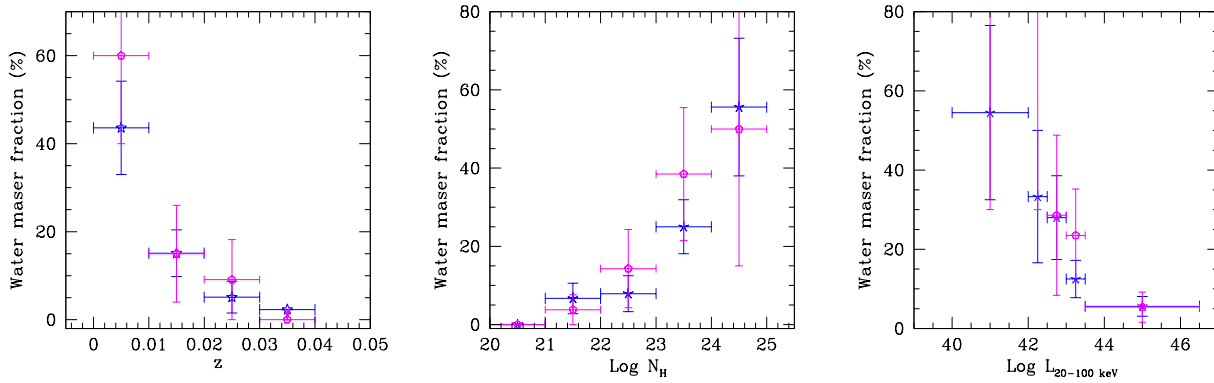


Fig. 2: Fraction of detected water maser emission versus redshift limited to $z < 0.04$, X-ray column density in cm^{-2} (central panel) and 20-100 keV luminosity in $\text{ergs s}^{-1} \text{cm}^{-2}$ (right panel). Blue starred points represent the total sample, magenta polygons are for the complete sub-sample.

sources may affect this result: a decline of the detection fraction is seen going from low to high luminosities, maybe an indication that an extremely luminous nuclear environment does not favour maser emission. Indeed, as discussed in Castangia et al. (2013, and references therein), for large nuclear bolometric luminosities or environments particularly exposed to strong X-ray radiation, H_2O maser emission at sub-parsec distances from the nucleus of the galaxy may be hampered because the interstellar medium is mostly atomic and/or the dust grains (where water is thought to be often formed) are destroyed. If this scenario is correct, while maser emission can still be produced at larger distances, the innermost (hundredths of parsecs) masing action would be prevented. In addition, an increased bolometric luminosity might decrease the maser emissivity by reducing the difference between gas and dust temperatures (Kuo et al. 2018), from which the volume rate of maser photon production significantly depends (Gray et al. 2016).

Fractions for the total and the complete sub-samples are consistent within errors and trends are confirmed for the two samples. However, the statistics is limited by the small number of data sets, especially for the complete sub-sample.

6. Maser type of INTEGRAL AGN

Most maser detections reported in this work have been discussed in the literature and their maser type analysed in previous works (see type and relative references in the notes of Table 1A). In the following and in Table 1A, we have considered as disk, outflow or jet maser, sources for which the maser class is either fully assessed or just suggested on the basis of observational results; for these last objects only follow-up, mainly interferometric VLBI, continuum and spectral line studies can confirm water maser association with AGN activity and maser type.

Only 6 sources in the sample of 29 maser detections (IGR J05081+1722, NGC 3081, NGC 3783, NGC 5643, NGC 6300 and ESO 103-G35) have no associated maser classification; in Appendix B we attempt to provide some indication on the possible nature of these sources and implicitly discuss their most likely maser type. As seen from Table 1A water maser classification generally refer to one or, in some case, two components, such as disc plus outflow or jet.

Excluding these 6 sources from our sample of AGN with 22 GHz detection, we notice that similar numbers (12-12) of objects have disc (or evidence of disc) and jet (or evidence of jet) water emission; outflow or evidence of outflow emission is present in 7 sources. Despite the uncertainties involved in water maser classification, it is evident from the present sample that all types of masers are likely associated to INTEGRAL AGN and that discs masers are not necessarily the dominant type. Thus hard X-ray surveys offer also the opportunity to probe masers of different types.

Finally we note that all optical narrow line AGN (including type 1 and NLSy1) have maser type likely related to jet and/or outflows emission and none is apparently associated to accretion discs. Type 2 AGN instead seem to display all types of water maser: out of 24 Seyfert 2 detected, 12 have emission partly or totally associated to a disc, 8 to a jet and only 3 to outflow. Maser sources associated to edge-on ($i = 90 \pm 10$ degrees, see Sect. 8) discs are most likely, and not surprisingly according to the Unified Model, found in type 2 AGN.

7. Maser vs non maser INTEGRAL AGN

One main question still unanswered in extragalactic maser astrophysics is related to the conditions that lead to maser emission in only a fraction of AGN; it is therefore reasonable to ask whether water maser galaxies have special intrinsic properties in terms of X/hard X-ray luminosities and absorption, relative to apparently similar galaxies without detected maser emission.

According to theory, high energy radiation coming from the central part of an AGN could heat the circumnuclear gas temperature to values suitable for maser emission (Neufeld et al. 1994); in this case, we expect a relationship between the maser luminosity and the X-ray/hard X-ray luminosities. Indeed Kondratko et al. (2006b), studying a sample of 30 water masers AGN found such a relation ($L_X \propto L_{\text{H}_2\text{O}}^{0.5}$), where L_X is the unabsorbed X-ray luminosity in the 2–10 keV band; the significance of such correlation improved by limiting the sample to disc masers only. However, the relation still presented a large scatter, likely due to a dependence from different parameters, such as the mass accretion rate, the ratio of X-ray to bolometric luminosity and the well known X-ray and maser variability (in the latter typically of the order of tens of per cent, e.g., Maloney 2002 and references

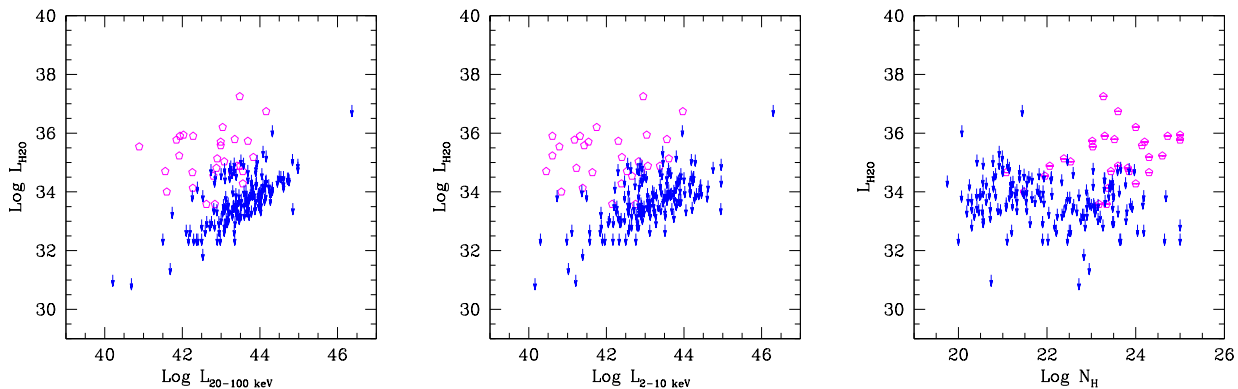


Fig. 3: Logarithmic water maser luminosity versus 20–100 keV (left panel) and 2–10 keV logarithmic luminosities (central panel), expressed in $\text{ergs s}^{-1} \text{cm}^{-2}$. Water maser luminosity versus the logarithmic X-ray column density in cm^{-2} (right panel). Magenta empty polygons are water maser detected sources, blue arrows represent water maser luminosity upper limits.

therein). Indeed, this relation seems to be weak or absent in more recent studies even considering only disc maser sources, i.e. those in which the correlation is expected to be stronger (Castangia et al. 2013).

A more direct estimate of the AGN radiation field is provided by the hard X-ray luminosity, which is the least affected in terms of nuclear absorption; this information is available for all our objects and has never been employed before in a correlation with the maser luminosity. In Fig. 3 (left and middle panels) we therefore plot the isotropic water maser luminosity as a function of both 20–100 keV and 2–10 keV observed luminosities. Applying the regression analysis to only the detected sources, the Spearman’s Rho correlation coefficients result in 0.16 and 0.10, providing a 2-tailed probability of 0.42 and 0.59 respectively, therefore the association between the two variables should not be considered statistically significant. The sources of scatter as discussed in Kondratko et al. (2006b) analogously applies to our relations.

Finally we note here too that the range of hard X-ray and X-ray luminosities of detected maser cover a similar interval as non maser AGN, therefore no evident luminosity threshold could be identified as maser activator above $L_{2-10\text{keV}} \sim 10^{40} \text{ ergs s}^{-1}$. In addition, the sensitivity of 22 GHz surveys is not a limit for maser detection since luminosity upper limits are also found at a factor of ~ 10 to 100 below detections.

As discussed by Zhang et al. (2006), a correlation between water maser luminosity and X-ray absorption (roughly $L_{\text{H}_2\text{O}} \propto N_{\text{H}}^3$) is also expected for idealized saturated maser emission (assuming no velocity gradients in the maser region). In this case the value of the exponent is determined by the luminosity increasing linearly with the column density and the surface of the masing cone growing with the square of its lengths (e.g., Kylafis & Norman 1991). In Fig. 3 (right panel), we display the isotropic water maser luminosity as a function of the X-ray absorption for maser and non maser sources; again considering only detected sources, the resulting Spearman’s Rho correlation coefficients is 0.37 with a derived 2-tailed probability of 0.05, suggesting that the association between the two variables could be considered statistically significant only marginally. Again confirming that the X-ray obscuring medium is associated with the masing material.

While an interpretation based on the different maser types would be interesting, this, given the variety of maser types in our sources, would reduce the number of sources tested, weakening the significance of such relations. In addition, the large complexity of the different maser components introduces a source of difficulty in the interpretation of such correlations.

8. Water masers in Compton thick AGN

Of the 21 objects of the total sample in the CT regime, 8 have no maser detection, 10 have maser detection and 3 have not been observed yet. Therefore we have a roughly $56 \pm 18\%$ chance of detecting maser emission in the Compton thick AGN set selected in the hard X-ray band (see also Sect. 5). This is in line with the noticeably large fraction of water masers (50%) found by Castangia et al. (2019) studying a sample of heavily absorbed AGN, including CT sources, selected through a combination of mid-IR and X-ray data. We note that all CT AGN in the INTEGRAL sample show evidence of an association with discs (sometimes accompanied by jet and outflow components), except for Mkn 3 which is tentatively associated to a jet origin only (indeed a core plus jet component is seen in the radio continuum maps of this source, Chiaraluce et al. 2020). If we exclude Mkn 3, the fraction of disc masers in CT is $50 \pm 17\%$. What is interesting here is why some sources are able to develop strong maser emission while others are not, in other words if all Compton thick AGN are potentially water maser emitters, the question is why only half are able to reach luminosities high enough (above $10^{33} \text{ erg cm}^{-2} \text{ s}^{-1}$, see Fig. 3) for the current generation of radio receivers.

Masini & Comastri (2017) have estimated the expected disc water maser detection fraction among type 2 Seyferts in a volume-limited survey to be of about 10% to 20%. This value has been obtained by comparing the torus and maser discs covering factors (see their equation 2.1) and assuming that a maser disc is detected if the line of sight angle ranges between $90 \pm 10^\circ$ with respect to the polar axis and defining the probability of detecting a maser disc in a type 2 AGN as the ratio of the maser disc covering factor with respect to the torus one. We could invert such assumption considering a covering factor for the CT part of the torus as derived from X-ray arguments (Ricci 2017) to be $\sim 23\%$ (also in agreement with IR arguments, e.g., Hönig 2019) and using the information on the ratio between the water

maser and CT covering factors to be 50%, to finally derive the expected maser disc inclination angle to range between 82 and 87°. These values are in agreement with the observed disc angles in well known disc masers (Kuo et al. 2011; König et al. 2012), confirming the idea that the masing disc is only a portion of the total CT medium (for a sketch of the possible geometry discussed here see Fig. 2 in Masini et al. 2016). The maser covering factor could be considered as a lower limit if we assume the presence of warped discs that should increase the probability of intercepting maser emission (Darling 2017). Similarly, the known water maser variability could contribute to a possible non detection if the masers flux goes below the instrument sensitivity and therefore to an underestimate of the covering factor. Other effects contribute to our uncertainties in these estimates, for instance X-ray scattering in clumpy media could dilute the true line-of-sight column density, and thus prevents us from deriving unbiased orientation information (Ramolla et al. 2011). Despite the uncertainties involved, it is important to stress that the 50% detection fraction in Compton thick AGN can, in principle, be explained in terms of a geometrical effect (i.e. proper opening angles of torus and maser disc and their relative alignment) and may not be due to peculiarities of individual objects.

9. Conclusions

Notwithstanding the valuable science that can be derived for AGN and cosmological studies, water megamasers are rarely found in galaxies surveys (e.g., Braatz et al. 2018). In this work, we have selected a sample of hard X-ray AGN detected above 20 keV by INTEGRAL/IBIS and searched for water megamaser emission among them, both in literature and through our new dedicated observations (where one new maser detection has been obtained). Among the 380 sources belonging to the sample, only 51% have been observed at 22 GHz and in $15 \pm 3\%$ of them a detection has been found. We have also considered a sub-sample of 87 sources, limited in volume and statistically complete, finding that the detection fraction raises up to $19 \pm 5\%$. The majority of the observed sources are at low redshift and this is reflected by the observed detection fraction that decreases with increasing redshift, likely introducing a bias in our sample.

So far, the detection rates observed in large surveys of optically selected galaxies were around a few percent, boosted only by carefully selecting smaller samples on the basis of IR (8-22%; Hagiwara et al. 2002, 2003; Henkel et al. 2005) or a combination of mid-IR and X-ray data (50%; Castangia et al. 2019). Therefore, the hard X-ray selection provides among the highest rates ever observed so far.

These fractions increase in type 2 Seyfert galaxies ($22 \pm 5\%$), in particular in CT AGN where $\sim 50\%$ of them host water maser discs. This clearly indicates that the X-ray obscuring gas is related to the maser dusty medium. A comparison between the covering factor of the CT obscuring medium and the fraction of water masers in CT sources confirms the idea that the masing disc is possibly only a portion of the CT obscuring medium and that an edge-on line of sight ($i > 82^\circ$) is required for the water maser emission to be detected.

A possible decline of the detection fraction is observed as the hard X-ray luminosity increases, suggesting that a high luminous nuclear environment might not favour maser emission. However, this result can be confirmed by completing the sample observations at higher luminosity. On the other hand, no significant correlation between the water maser and X-ray and hard X-ray luminosities has been found, while the marginally significant correlation between the water maser luminosity and the X-

ray column density simply reflects the connection between the X-ray obscuring and the masing media.

All types of water masers are found by the soft-gamma ray selection of sources. Interestingly, of the few water masers detected in type 1 AGN, all of them are jet/outflow candidates, while in type 2 AGN all type of masers are detected, suggesting that the dusty water maser medium is not solely associated with a classical obscuring torus, but could also reside in polar outflows/jets, implying a more complex geometry as envisaged by recent IR interferometric studies (see Hönig et al. 2018).

Overall we can conclude that hard X-ray samples of AGN provide the opportunity to enhance significantly maser detection efficiency over previous surveys, reaching extremely high detection fractions (up to 50%) by targeting type 2/heavily absorbed AGN which are nearby and in an optimized luminosity range. The discovery of new heavily absorbed sources with the increased sensitivity of the ongoing INTEGRAL/IBIS and Swift/BAT surveys together with the wealth of new sources that the eROSITA survey (Merloni 2018) will discover below 10 keV will offer the possibility to largely increase the samples for future water maser searches and, hopefully, detections.

Acknowledgements

AT and PC would like to thank Jim Braatz for providing information on some of the maser sources, prior to publication. FP, AM, LB, AB and PU acknowledge financial support from ASI under contract INTEGRAL ASI/INAF n.2019-35-HH. We acknowledge the help of 3 high school students (Alice Bizzarri, Andrea Coccozza and Fulvio Talarico) in the analysis of the BAT 70 m sample; they all participated in a summer stage at OAS/INAF Bologna during 2016. This project, being partly conducted by amateur astronomers under the supervision of professional scientists, represents a nice example on how citizen science work can help in dealing with a large data set.

References

- Alonso-Herrero, A., Pereira-Santaella, M., García-Burillo, S., et al. 2018, *ApJ*, 859, 144
- Antonucci, R. R. J., & Miller, J. S. 1985, *ApJ*, 297, 621
- Ballo, L., Severgnini, P., Braito, V., et al. 2015, *A&A*, 581, A87
- Baumgartner, W. H., Tueller, J., Markwardt, C. B., et al. 2013, *ApJS*, 207, 19
- Bennert, N., Schulz, H., & Henkel, C. 2004, *A&A*, 419, 127
- Bennert, N., Barvainis, R., Henkel, C., et al. 2009, *ApJ*, 695, 276
- Bird, A. J., Malizia, A., Bazzano, A., et al. 2007, *ApJS*, 170, 175
- Bird, A. J., Bazzano, A., Malizia, A., et al. 2016, *ApJS*, 223, 15
- Braatz, J., Pesce, D., Condon, J., et al. 2018, *Science with a Next Generation Very Large Array*, 821
- Braatz, J. A., Reid, M. J., Greenhill, L. J., et al. 2008, *Frontiers of Astrophysics: A Celebration of Nrao's 50th Anniversary*, 103
- Braatz, J. A., & Gugliucci, N. E. 2008, *ApJ*, 678, 96
- Braatz, J. A., Wilson, A. S., & Henkel, C. 1997, *ApJS*, 110, 321
- Braatz, J. A., Reid, M. J., Humphreys, E. M. L., et al. 2010, *ApJ*, 718, 657
- Braatz, J. 2008, *A Decade of Dark Energy*, 5
- Braatz, J., Condon, J., Constantin, A., et al. 2015, *IAU General Assembly* 29, 2255730
- Castangia, P., Surcis, G., Tarchi, A., et al. 2019, *A&A*, 629, A25
- Castangia, P., Panessa, F., Henkel, C., et al. 2013, *MNRAS*, 436, 3388
- Darling, J. 2017, *ApJ*, 837, 100
- Davies, R. I., Maciejewski, W., Hicks, E. K. S., et al. 2014, *ApJ*, 792, 101
- Decarli, R., Dotti, M., Fontana, M., et al. 2008, *MNRAS*, 386, L15
- Diamond-Stanic, A. M., Rieke, G. H., & Rigby, J. R. 2009, *ApJ*, 698, 623
- Elitzur, M., & Shlosman, I. 2006, *ApJ*, 648, L101
- Elitzur, M. 1992, *Astrophysics and Space Science Library*
- Gallimore, J. F., Henkel, C., Baum, S. A., et al. 2001, *ApJ*, 556, 694
- Gallimore, J. F., Baum, S. A., O'Dea, C. P., et al. 1996, *ApJ*, 458, 136
- Gear, W. K., Stevens, J. A., Hughes, D. H., et al. 1994, *MNRAS*, 267, 167
- Gehrels, N., Chincarini, G., Giommi, P., et al. 2004, *ApJ*, 611, 1005
- Gofford, J., Reeves, J. N., McLaughlin, D. E., et al. 2015, *MNRAS*, 451, 4169

- Gray, M. D., Baudry, A., Richards, A. M. S., et al. 2016, *MNRAS*, 456, 374
- Greenhill, L. J., Ellingsen, S. P., Norris, R. P., et al. 2002, *ApJ*, 565, 836
- Greenhill, L. J., Kondratko, P. T., Lovell, J. E. J., et al. 2003a, *ApJ*, 582, L11
- Greenhill, L. J., Booth, R. S., Ellingsen, S. P., et al. 2003b, *ApJ*, 590, 162
- Greenhill, L. J., Tilak, A., & Madejski, G. 2008, *ApJ*, 686, L13
- Greenhill, L. J., Kondratko, P. T., Moran, J. M., et al. 2009, *ApJ*, 707, 787
- Hagiwara, Y., Diamond, P. J., & Miyoshi, M. 2002, *A&A*, 383, 65
- Hagiwara, Y., Diamond, P. J., Miyoshi, M., et al. 2003, *MNRAS*, 344, L53
- Hagiwara, Y., & Edwards, P. G. 2015, *ApJ*, 815, 124
- Henkel, C., Guesten, R., Downes, D., et al. 1984, *A&A*, 141, L1
- Henkel, C., Peck, A. B., Tarchi, A., et al. 2005, *A&A*, 436, 75
- Herrnstein, J. R., Moran, J. M., Greenhill, L. J., et al. 1997, *ApJ*, 475, L17
- Humphreys, E. M. L., Vlemmings, W. H. T., Impellizzeri, C. M. V., et al. 2016, *A&A*, 592, L13
- Hönig, S. F., Alonso Herrero, A., Gandhi, P., et al. 2018, *Experimental Astronomy*, 46, 413
- Jarosik, N., Bennett, C. L., Dunkley, J., et al. 2011, *ApJS*, 192, 14
- Kamali, F., Henkel, C., Brunthaler, A., et al. 2017, *A&A*, 605, A84
- Kamenno, S., Nakai, N., Sawada-Satoh, S., et al. 2005, *ApJ*, 620, 145
- Kondratko, P. T., Greenhill, L. J., & Moran, J. M. 2005, *ApJ*, 618, 618
- Kondratko, P. T., Greenhill, L. J., Moran, J. M., et al. 2006a, *ApJ*, 638, 100
- Kondratko, P. T., Greenhill, L. J., & Moran, J. M. 2006b, *ApJ*, 652, 136
- Kuo, C. Y., Constantin, A., Braatz, J. A., et al. 2018, *ApJ*, 860, 169
- Kuo, C. Y., Braatz, J. A., Condon, J. J., et al. 2011, *ApJ*, 727, 20
- Kylafis, N. D., & Norman, C. A. 1991, *ApJ*, 373, 525
- König, S., Eckart, A., Henkel, C., et al. 2012, *MNRAS*, 420, 2263
- Leipski, C., Falcke, H., Bennert, N., et al. 2006, *A&A*, 455, 161
- Liu, Z. W., Zhang, J. S., Henkel, C., et al. 2017, *MNRAS*, 466, 1608
- Lo, K. Y. 2005, *ARA&A*, 43, 625
- Malizia, A., Landi, R., Molina, M., et al. 2016, *MNRAS*, 460, 19
- Malizia, A., Bassani, L., Bazzano, A., et al. 2012, *MNRAS*, 426, 1750
- Malizia, A., Stephen, J. B., Bassani, L., et al. 2009, *MNRAS*, 399, 944
- Maloney, P. R. 2002, *PASA*, 19, 401
- Masini, A., Comastri, A., Baloković, M., et al. 2016, *A&A*, 589, A59
- Masini, A., & Comastri, A. 2018, *Astrophysical Masers: Unlocking the Mysteries of the Universe*, 133
- Mathur, S. 2000, *MNRAS*, 314, L17
- Mehdipour, M., Kaastra, J. S., Kriss, G. A., et al. 2017, *A&A*, 607, A28
- Merloni, A. 2018, *AGN13: Beauty and the Beast*, 71
- Miyoshi, M., Moran, J., Herrnstein, J., et al. 1995, *Nature*, 373, 127
- Morganti, R., Tsvetanov, Z. I., Gallimore, J., et al. 1999, *A&AS*, 137, 457
- Neufeld, D. A., Maloney, P. R., & Conger, S. 1994, *ApJ*, 436, L127
- Oh K., et al., 2018, *ApJS*, 235, 4
- Orienti, M., & Prieto, M. A. 2010, *MNRAS*, 401, 2599
- Ott, J., Meier, D. S., McCoy, M., et al. 2013, *ApJ*, 771, L41
- Padovani, P., Alexander, D. M., Assef, R. J., et al. 2017, *A&A Rev.*, 25, 2
- Panessa, F., de Rosa, A., Bassani, L., et al. 2011, *MNRAS*, 417, 2426
- Peck, A. B., Henkel, C., Ulvestad, J. S., et al. 2003, *ApJ*, 590, 149
- Pesce, D. W., Braatz, J. A., Condon, J. J., et al. 2015, *ApJ*, 810, 65
- Ramolla, M., Haas, M., Bennert, V. N., et al. 2011, *A&A*, 530, A147
- Reid, M. J., Braatz, J. A., Condon, J. J., et al. 2009, *ApJ*, 695, 287
- Ricci, C., Trakhtenbrot, B., Koss, M. J., et al. 2017, *Nature*, 549, 488
- Sato, N., Yamauchi, A., Ishihara, Y., et al. 2005, *PASJ*, 57, 587
- Schnorr-Müller, A., Storchi-Bergmann, T., Robinson, A., et al. 2016, *MNRAS*, 457, 972
- Tarchi, A., Henkel, C., Chiaberge, M., et al. 2003, *A&A*, 407, L33
- Tarchi, A., Castangia, P., Henkel, C., et al. 2011a, *A&A*, 525, A91
- Tarchi, A., Castangia, P., Columbano, A., et al. 2011b, *A&A*, 532, A125
- Tarchi, A. 2012, *Cosmic Masers - from OH to H0*, 323
- Tilak, A., Greenhill, L. J., Done, C., et al. 2008, *ApJ*, 678, 701
- Tueller, J., Mushotzky, R. F., Barthelmy, S., et al. 2008, *ApJ*, 681, 113
- Ubertini, P., Lebrun, F., Di Cocco, G., et al. 2003, *A&A*, 411, L131
- van den Bosch, R. C. E., Greene, J. E., Braatz, J. A., et al. 2016, *ApJ*, 819, 11
- Vulic, N., Hornschemeier, A. E., Wik, D. R., et al. 2018, *ApJ*, 864, 150
- Wang, J., Zhang, J.-S., & Fan, J.-H. 2010, *Research in Astronomy and Astrophysics*, 10, 915
- Yamashita, T., Komugi, S., Matsuhara, H., et al. 2017, *ApJ*, 844, 96
- Zhang, J. S., Henkel, C., Guo, Q., et al. 2012, *A&A*, 538, A152
- Zhang, J. S., Liu, Z. W., Henkel, C., et al. 2017, *ApJ*, 836, L20
- Zhang, J. S., Henkel, C., Kadler, M., et al. 2006, *A&A*, 450, 933
- Zhu, G., Zaw, I., Blanton, M. R., et al. 2011, *ApJ*, 742, 73

Table .1: Table 1A: Galaxies detected by *INTEGRAL*/IBIS.

Name	RA	Dec	z	Class	F_{HX}^+	F_X^+	$\log N_H$	Notes	Rms*	L_{H2O}^{**}	Ref.***
IGR J00040+7020	00 04 01.92	+70 19 18.5	0.096	Sy2	1.47	0.35	22.52				
IGR J00158+5605	00 15 54.19	+56 02 57.5	0.169	Sy1.5	<0.66	0.31	21.50				
IGR J00256+6821	00 25 32.50	+68 21 44.0	0.012	Sy2	1.47	0.05	23.60				
IGR J00333+6122	00 33 18.34	+61 27 43.3	0.105	Sy1.5	1.38	0.68	21.93	O	2	<14.0	this work
SWIFT J0034.5-7904	00 34 16.7	-79 05 20	0.07400	Sy1	1.09	6.33	23.49				
IES 0033+595	00 35 52.60	+59 50 05.0	0.086	BL Lac	1.83	5.90	21.55	O	2	<9.4	this work
IGR J00465-4005	00 46 20.68	-40 05 49.1	0.201	Sy2	3.56	0.12	23.38				
MKN 348	00 48 47.10	+31 57 25.0	0.015	Sy2	10.60	0.44	23.02	M(J,a)		142±28	P03
Mrk 352	00 59 53.3	+31 49 37	0.01486	Sy1	3.21	11.89	20.72	O	4	<0.6	MCP
Mrk 1152	01 13 50.1	-14 50 44	0.05271	Sy1.5	2.94	4.66	20.25	O	4	<7.0	MCP
Fairall 9	01 23 45.8	-58 48 21	0.04702	Sy1.2	3.34	7.40	20.50				
NGC 526A	01 23 54.40	-35 03 56.0	0.019	Sy1.9	5.34	1.80	22.23	O	3	<0.7	MCP
RX J0137.7+5814	01 37 50.49	+58 14 11.0	-	BL Lac	<0.68	1.01	21.60				
ESO 297-18	01 38 37.10	-40 00 41.0	0.025	Sy2	6.08	0.33	23.70	O	16(1.3)	<27.4	K06
IGR J01528-0845	01 52 48.4	-08 43 21	0.03697	Sy2 ^s	0.85	0.40	23.49	O	4	<3.5	MCP
IGR J01528-0326	01 52 49.00	-03 26 48.5	0.017	Sy2	2.60	0.40	23.15	O	3	<0.5	MCP
IGR J01545+6437	01 54 35.29	+64 37 57.5	0.034	Sy2	<0.83	0.0097	21.82	O	6	<4.4	MCP
Mrk 584	02 00 26.3	+02 40 10	0.07877	Sy1.8	1.79	3.98	20.47				
NGC 788	02 01 06.40	-06 48 56.0	0.0136	Sy2	6.00	0.61	23.48	O	3	<0.4	MCP
Mrk 1018	02 06 16.00	-00 17 29.0	0.0424	Sy1	1.70	1.19	20.41	O	3	<3.4	MCP
IGR J02086-1742	02 08 34.95	-17 39 34.8	0.129	Sy1.2	2.75	0.64	<20.23				
IGR J02097+5222	02 09 34.30	+52 22 48.0	0.0492	Sy1	2.81	1.30	21.23	O	6	<9.2	MCP
Mrk 590	02 14 33.50	-00 46 00.0	0.02638	Sy1	1.46	0.64	20.42	O	3	<1.3	MCP
SWIFT J0216.3+5128	02 16 26.73	+51 25 25.1	0.422	Sy2 ?	1.62	1.27	22.104				
SWIFT J0218.0+7348	02 17 30.83	+73 49 32.5	2.367	QSO/bl	2.70	0.55	21.54				
Mrk 1040	02 28 14.50	+31 18 42.0	0.0166	Sy1.5	5.19	0.51	20.56	O	3	<0.5	MCP
IGR J02341+0228	02 33 49.0	+02 29 25	0.32100	QSO	1.55	2.90	20.40				
IGR J02343+3229	02 34 20.10	+32 30 20.0	0.0162	Sy2/L	4.74	0.82	22.34	O	4	<0.7	MCP
NGC 985	02 34 37.80	-08 47 15.0	0.043	Sy1.5	2.38	5.40	20.50	O	3	<3.5	MCP
NGC 1052	02 41 04.80	-08 15 21.0	0.005	Sy2/L	1.69	0.40	23.30	M(J,a)		208±16	K05
RBS 345	02 42 14.60	+05 30 36.0	0.069	Sy1	2.02	0.26	20.72				
NGC 1068	02 42 40.70	-00 00 48.0	0.0038	Sy2	2.36	0.50	25.00	M(D+J,a)		155±5	G96
QSO B0241+62	02 44 57.69	+62 28 06.5	0.044	Sy1.2	5.17	3.6	21.32	O	4	<4.9	MCP
MCG -07-06-018	02 46 37.00	-42 22 01.0	0.0696	XBONG	3.72	0.007	>24				
SWIFT J0249.1+2627	02 48 59.3	+26 30 39	0.05800	Sy2	1.90	3.73	23.43	O	3	<6.4	MCP
IGR J02504+5443	02 50 42.59	+54 42 17.7	0.015	Sy2	1.87	0.48	21.62	O	3	<0.4	MCP
MCG -02-08-014	02 52 23.40	-08 30 37.0	0.0167	Sy2?	1.88	1.20	23.08	O	5	<0.9	MCP
NGC 1142	02 55 12.20	-00 11 01.0	0.0288	Sy2	6.12	0.42	23.80	O	2	<1.0	MCP
MCG-02-08-038	03 00 04.3	-10 49 29	0.03259	Sy1	1.81	16.7	21.56				
NGC 1194	03 03 49.10	-01 06 13.0	0.0136	Sy2	2.57	0.09	24.20	M(D,a)		131±7	P15
PKS 0312-770	03 11 55.2	-76 51 51	0.22519	Sy1/QSO	1.21	2.19	20.93				
B3 B0309+411B	03 13 01.96	+41 20 01.2	0.136	Sy1	<2.49	2.36	21.11	O	3	<35.1	this work
SWIFT J0318.7+6828	03 18 19.02	+68 29 32.1	0.0901	Sy1.9	<0.91	0.73	22.61				
NGC 1275	03 19 48.16	+41 30 42.1	0.0175	Sy1.5/L	3.82	1.23	21.08	O	9	<1.7	MCP

Table .1: continue

Name	RA	Dec	z	Class	F_{HX}^+	F_X^-	Log N_H	Notes	Rms*	L_{H2O}^{**}	Ref.**
IH 0323+342	03 24 41.16	+34 10 45.8	0.061	NLSy1	3.96	0.64	21.16				
IGR J03249+4041-SW	03 25 13.20	+40 41 55.0	0.0477	Sy2	1.35	0.12	>21.18				
IGR J03249+4041-NE	03 25 12.20	+40 42 02.0	0.0475	Sy2	1.35	0.09	22.48				
IGR J03334+3718	03 33 18.79	+37 18 11.1	0.05583	Sy1.5	2.61	0.61	21.15				
NGC 1365	03 33 36.31	-36 08 27.8	0.0054	Sy1.9	4.10	1.30	24.65	O	3	<0.1	MCP
NRAO 140	03 36 30.10	+32 18 29.0	1.2580	QSO/bl	2.46	0.72	21.10				
ESO 548-G81	03 42 03.7	-21 14 40.0	0.0145	Sy1	4.45	1.35	20.36	O	5	<0.7	MCP
IGR J03532-6829	03 52 57.00	-68 31 18.0	0.087	BL Lac	<8.52	1.75	20.95	O	5	<1.1	MCP
SWIFT J0353.7+3711	03 53 42.5	+37 14 07	0.01865	Sy2/L	0.89	3.50	22.57				
4C +62.08	03 55 40.2	+62 40 59	1.10900	Sy1	1.30	0.45	21.51				
SWIFT J0357.6+4153	03 57 45.1	+41 55 05	0.05300	Sy1.9	1.55	5.88	22.30				
3C 098	03 58 55.00	+10 26 24.0	0.0304	Sy2	3.96	0.27	23.08	O	2	<1.2	MCP
4C03.8	04 07 16.45	+03 42 25.9	0.089	Sy2	3.45	0.21	23.45				
3C 111	04 18 21.28	+38 01 35.8	0.0485	Sy1	10.40	3.51	21.66	O	8	<11.9	this work
IGR J04221+4856	04 22 00.50	+48 56 04.0	0.114	Sy1	1.42	-	21.85				
LEDA 15023	04 23 40.80	+04 08 03.0	0.045	Sy2	1.87	0.13	23.48	O	6	<7.7	MCP
3C120	04 33 11.09	+05 21 15.6	0.033	Sy1.5	7.98	4.60	21.20	O	6	<4.1	MCP
UGC 3142	04 43 46.89	+28 58 19.0	0.0216	Sy1	4.87	1.70	22.60	O	5	<1.5	MCP
SWIFT J0444.1+2813	04 44 09.0	+28 13 01	0.01127	Sy2	1.49	12.34	22.53	O	3	<0.2	MCP
SWIFT J0450.7-5813	04 51 44.0	-58 11 01	0.09070	Sy1.5	1.85	4.74	20.95				
MCG -01-13-025	04 51 41.5	-03 48 33	0.01589	Sy1.2	1.47	21.3	20.54	O	6	<1.0	MCP
LEDA 168563	04 52 04.79	+49 32 44.6	0.029	Sy1	5.55	4.52	21.73	O	4	<2.1	MCP
SWIFT J0453.4+0404	04 53 25.74	+04 03 41.6	0.0296	Sy2	2.19	0.20	24.16	O	3	<1.7	MCP
ESO 033-G02	04 55 59.05	-75 32 28.3	0.0181	Sy2	2.42	1.59	22.10	O	15 (1.3)	<13.5	K06
LEDA 075258	05 02 09.00	+03 31 50.0	0.01599	Sy1	1.26	0.55	19.75	O	59	<9.5	B96
SWIFT J0505.8-2348	05 05 45.70	-23 51 14.0	0.03504	Sy2	5.49	1.36	23.50	O	4	<3.1	MCP
IGR J05081+1722	05 08 19.7	+17 21 48	0.01750	Sy2	1.25	6.45	22.38	M(?)		35±10	MCP
4U 0517+17	05 10 45.50	+16 29 55.0	0.0179	Sy1.5	6.83	2.53	20.95	O	5	<1.0	MCP
SWIFT J0515.3+1854	05 15 19.8	+18 54 52	0.02349	Sy2	1.81	1.91	23.06	O	4	<1.4	MCP
Ark 120	05 16 11.48	-00 09 00.6	0.0327	Sy1	6.55	2.87	20.99	O	45 (0.66)	<67.0	B96
SWIFT J0516.3+1928	05 16 22.7	+19 27 11	0.02115	Sy2	1.53	1.80	22.64				
SWIFT J0519.5-3140	05 19 35.81	-32 39 28.0	0.0126	Sy1.5	4.34	0.34	23.42	O	4	<0.4	MCP
PICTOR A	05 19 49.69	-45 46 44.5	0.0351	Sy1/L	<3.36	1.13	20.78	O	14 (1.3)	<47.3	K06
PKS 0521-36	05 22 58.00	-36 27 31.0	0.0565	Sy1	2.19	1.10	20.55	O	5	<10.1	MCP
PKS 0528+134	05 30 56.42	+13 31 54.9	2.060	QSO/bl	1.50	2.57	21.38				
QSO J0539-2839	05 39 54.3	-28 39 56.0	3.1040	QSO/bl	1.74	0.17	21.20				
SWIFT J0544.4+5909	05 44 22.6	+59 07 36	0.06597	Sy1.9	2.00	5.25	22.26				
IGR J05470+5034	05 47 14.9	+50 38 25	0.03600	Sy2	1.19	1.40	23.18				
NGC 2110	05 52 11.38	-07 27 22.4	0.0078	Sy2	17.90	2.50	22.46	O	3	<0.1	MCP
MCG+08-11-011	05 54 53.63	+46 26 21.8	0.0205	Sy1.5	8.46	5.62	21.32	O	4	<1.1	MCP
4U 0557-385	05 58 02.05	-38 20 04.6	0.0339	Sy1.2	<2.76	2.00	22.11	O	5	<3.6	MCP
IRAS 05589+2828	06 02 09.70	+28 28 17.0	0.033	Sy1	4.02	1.64	21.66	O	4	<2.8	MCP
SWIFT J0601.9-8636	06 05 39.60	-86 37 54.0	0.0064	Sy2	2.59	0.11	24.00				
IGR J06058-2755	06 05 48.96	-27 54 40.1	0.0900	Sy1.5	1.98	0.66	20.38				

Table .1: continue

Name	RA	Dec	z	Class	F_{HX}^+	F_X^+	$\log N_H$	Notes	Rms*	L_{H2O}^{**}	Ref.***
Mrk 3	06 15 36.31	+71 02 14.9	0.0135	Sy2	9.53	0.65	24.00	M(J ² ,b)		5±5	MCP
IGR J06233-6436	06 23 07.70	-64 36 20.0	0.12889	Sy1	1.56	0.46	20.59				
IGR J06239-6052	06 23 45.61	-60 58 45.4	0.0405	Sy2	<0.98	0.32	23.28				
SWIFT J0623.8-3215	06 23 46.4	-32 13 00	0.02243	Sy2	1.94	1.16	23.91	O	4	<1.3	MCP
PKS 0637-752	06 35 46.5	-75 16 17	0.65300	QSO/bl	1.66	4.72	21.10				
SWIFT J0640.4-2554	06 40 11.69	-25 53 43.4	0.0248	Sy1.2	3.83	1.88	21.38	O	13 (1.3)	<21.9	K06
IGR J06415+3251	06 41 23.00	+32 55 39.0	0.01719	Sy2	4.74	0.33	23.20	O	3	<0.6	MCP
Mrk 6	06 52 12.36	+74 25 37.2	0.0188	Sy1.5	4.32	2.51	22.90	O	3	<0.7	MCP
IGR J06523+5334	06 52 31.41	+53 34 31.5	0.301	Sy1.2/QSO	<4.83	0.02	20.81				
SWIFT J0709.3-1527	07 09 12.3	-15 27 00	0.13900	BL Lac	<1.25	13.6	21.76				
IGR J07225-3810	07 22 22.4	-38 14 55	1.023	QSO/bl	2.08	0.58	21.33				
PKS 0723-008	07 25 50.6	-00 54 57	0.12800	BL Lac	1.58	4.97	21.10				
LEDA 96373	07 26 26.30	-35 54 21.0	0.0294	Sy2	2.25	0.05	22.84				
Mrk 79	07 42 32.8	+49 48 35	0.02219	Sy1.2	4.89	15.8	20.72	O	4	<1.2	MCP
IGR J07565-4139	07 56 19.62	-41 37 42.1	0.021	Sy2	1.43	0.32	21.86	O	10	<2.8	this work
IGR J07597-3842	07 59 41.82	-38 43 56.0	0.04	Sy1.2	3.51	2.37	21.78	O	5	<5.1	this work
ESO 209-12	08 01 57.60	-49 46 42.0	0.0405	Sy1.5	2.25	8.30	21.38				
Mrk 1210	08 04 05.8	+05 06 50	0.01350	Sy2	5.96	9.70	23.52	M(D,c)		160±30	MCP
PG0804+761	08 10 58.65	+76 02 42.5	0.1	Sy1	<1.53	1.00	20.70				
IGR J08190-3835	08 19 11.36	-38 33 10.5	0.009	Sy2	1.36	0.15	23.13				
FRL 1146	08 38 30.70	-35 59 35.0	0.0316	Sy1.5	2.10	1.26	21.45	O	7	<4.4	this work
QSO B0836+710	08 41 24.36	+70 53 42.1	2.172	QSO/bl	5.77	2.63	20.47				
SWIFT J0845.0-3531	08 45 21.4	-35 30 24	0.13700	Sy1.2	1.11	4.64	22.38				
IGR J08557+6420	08 55 12.54	+64 23 45.5	0.037	Sy2?	1.74	0.28	23.29	O	14	<12.1	MCP
IGR J08558+0814	08 55 58.60	+08 13 19.0	0.22	Sy1	<3.49	0.0065	20.67				
Mrk 18	09 01 58.4	+60 09 06	0.01109	Sy2	2.62	1.57	23.26	O	4	<0.3	MCP
IGR J09025-6814	09 02 39.46	-68 13 36.6	0.014	XBONG	1.96	0.92	22.90				
IGR J09026-4812	09 02 37.31	-48 13 33.9	0.0391	Sy1	2.42	0.46	22.34				
IRXS J090431.1-382920	09 04 33.3	-38 29 22	0.01603	Sy1	0.92	0.92	21.46				
SWIFT J0917.2-6221	09 16 09.41	-62 19 29.5	0.0573	Sy1	1.91	1.43	21.61				
IGR J09189-4418	09 18 58.8	-44 18 30	-	AGN	0.53	2.30	22.66				
MCG-01-24-012	09 20 46.31	-08 03 21.9	0.0196	Sy2	4.06	1.00	22.80	O	3	<0.7	MCP
Mrk 110	09 25 12.85	+52 17 10.5	0.0353	NLSy1	5.06	2.79	20.30	O	3	<2.3	MCP
IGR J09253+6929	09 25 47.56	+69 27 53.6	0.039	Sy1.5	<1.94	0.05	23.15				
SWIFT J0929.7+6232	09 29 37.8	+62 32 39	0.02561	Sy2	2.06	0.97	23.31	O	5	<2.1	MCP
IGR J09446-2636	09 44 37.02	-26 33 55.4	0.1425	Sy1.5	<2.34	0.5	20.81				
NGC 2992	09 45 42.05	-14 19 35.0	0.0077	Sy2	6.51	1.20	21.90	O	2	<0.1	MCP
MCG-05-23-016	09 47 40.17	-30 56 55.9	0.0085	Sy2	14.50	8.76	22.21	O	5	<0.2	MCP
4C 73.08	09 49 45.8	+73 14 23	0.05810	Sy2	1.17	1.81	23.96				
IGR J09523-6231	09 52 20.70	-62 32 37.0	0.252	Sy1.9	1.43	0.37	22.80				
M 81	09 55 33.2	+69 03 55	0.00084	Sy1.8/L	1.11	11.1	20.74	O	9	<0.004	MCP
NGC 3081	09 59 29.54	-22 49 34.6	0.0079	Sy2	5.91	0.13	23.82	M(?)		17±8	MCP
SWIFT J0959.7-3112	09 59 42.6	-31 12 58	0.03700	Sy1	2.21	7.18	20.80				
NGC 3079	10 01 57.8	+55 40 47	0.00372	Sy2	3.72	38.0	25.00	M(D+O,d)		230±40	MCP

Table .1: continue

Name	RA	Dec	z	Class	F_{HX}^+	F_X^+	Log N_H	Notes	Rms*	L_{H2O}^{**}	Ref.***
SWIFT J1009.3-4250	10 09 48.22	-42 48 40.4	0.033	Sy2	2.81	0.31	23.41	O	10	<6.9	this work
IGR J10147-6354	10 14 15.55	-63 51 50.1	0.202	Sy1.2	<1.07	0.21	22.30				
NGC 3227	10 23 30.61	+19 51 53.8	0.0038	Sy1.5	11.30	0.81	22.83	O	3	<0.03	MCP
NGC 3281	10 31 52.06	-34 51 13.3	0.0107	Sy2	5.11	0.29	24.18	O	3	<0.2	MCP
SWIFT J1038.8-4942	10 38 45.20	-49 46 53.2	0.06	Sy1.5	2.00	1.45	21.79				
IGR J10404-4625	10 40 22.55	-46 25 25.7	0.024	Sy2	3.36	1.20	22.61				
MCG+04-26-006	10 46 42.67	+25 55 52.5	0.02	L	3.19	0.22	23.09	O	4	<1.0	MCP
Mrk 421	11 04 27.31	+38 12 31.8	0.0300	BL Lac	37.65	47.9	20.89	O	2	<1.1	MCP
NGC 3516	11 06 47.50	+72 34 07.0	0.0088	Sy1.5	5.55	2.3	22.50	O	4	<0.2	MCP
IGR J11366-6002	11 36 42.04	-60 03 06.6	0.014	Sy2/L	1.02	0.46	22.40				
NGC 3783	11 39 01.78	-37 44 18.7	0.0097	Sy1.5	13.30	6.03	22.06	M(?)		20±5	MCP
SWIFT J1143.7+7942	11 45 16.0	+79 40 53	0.00652	Sy1.2	2.21	6.51	20.00	O	4	<0.1	MCP
H1143-182	11 45 40.47	-18 27 15.5	0.0329	Sy1.5	<4.89	1.43	20.48	O	5	<3.4	MCP
PKS 1143-696	11 45 53.62	-69 54 01.8	0.244	Sy1.2	1.36	0.54	21.21				
B2 1144+35B	11 47 22.1	+35 01 08	0.06313	Sy1.9	1.21	3.09	20.23				
SWIFT J1200.8+0650	12 00 57.92	+06 48 23.1	0.0360	Sy2	1.72	0.58	22.92	O	3	<2.5	MCP
IGR J12026-5349	12 02 47.63	-53 50 07.7	0.028	Sy2	3.72	0.85	22.41				
NGC 4051	12 03 09.62	+44 31 52.8	0.0023	NLSy1	3.59	0.63	21.48	M(J/O,e)		2.6±0.2	T11
NGC 4074	12 04 29.65	+20 18 58.2	0.0224	Sy2	2.19	0.18	23.48	O	4	<1.3	MCP
Mrk 198	12 09 14.1	+47 03 30	0.02422	Sy2	1.09	5.12	23.00	O	4	<1.5	MCP
NGC 4138	12 09 29.79	+43 41 07.1	0.0030	Sy1.9	2.62	0.554	22.95	O	2	<0.01	MCP
NGC 4151	12 10 32.66	+39 24 20.7	0.0033	Sy1.5	30.50	25.00	23.34	M(J?,b)		1.0±0.5	MCP
IGR J12107+3822	12 10 44.27	+38 20 10.1	0.0229	Sy1.5	1.47	0.34	22.67	O	3	<1.0	MCP
IGR J12131+0700	12 12 49.81	+06 59 45.1	0.2095	Sy1.5-1.8	1.74	0.013	20.14				
NGC4235	12 17 09.91	+07 11 28.3	0.0080	Sy1.2	<0.94	0.28	21.20	O	6	<0.2	MCP
Mrk 766	12 18 26.48	+29 48 46.2	0.0129	NLSy1	1.81	1.33	21.95	M(J/O?,e)		9.1±0.7	T11
NGC 4258	12 18 57.5	+47 18 14.0	0.00149	Sy2	1.69	1.35	23.03	M(D,a)		89.7±0.2	P15
PKS 1217+02	12 20 11.9	+02 03 42	0.24023	Sy1.2	1.02	4.3	20.25				
PG 1218+305	12 21 21.9	+30 10 37	0.18365	BL Lac	0.92	0.26	20.29				
4C 04.42	12 22 22.55	+04 13 15.8	0.965	QSO/bl	2.30	0.25	20.23				
Mrk 50	12 23 24.14	+02 40 44.8	0.0234	Sy1	<1.30	0.98	<21.08	O	4	<1.4	this work
PG 1222+216	12 24 54.4	+21 22 46	0.43200	QSO/bl	1.64	8.30	20.32				
NGC 4388	12 25 46.93	+12 39 43.3	0.0084	Sy2	24.60	2.30	23.44	M(D,a)		13±3	P15
NGC 4395	12 25 48.93	+33 32 47.8	0.00106	Sy2	2.090	0.62	22.72	O	4	<0.003	MCP
IGR J12288+0052	12 28 45.70	+00 50 19.0	0.5756	Sy2	<0.92	0.03	22.40				
3C 273	12 29 06.70	+02 03 08.6	0.1583	Sy1/QSO	19.46	9.62	20.23				
IGR J12319-0749	12 31 57.7	-07 47 18	3.66800	QSO/bl	0.98	5.70	20.23				
Mrk 771	12 32 03.6	+20 09 29	0.06301	Sy1	0.83	3.01	20.44				
XSS J12303-4232	12 32 11.8	-42 17 52	0.10000	Sy1.5	1.36	5.40	20.88				
NGC 4507	12 35 36.55	-39 54 33.3	0.0118	Sy2	16.30	1.28	23.88	O	10	<0.9	MCP
ESO 506-G27	12 38 54.40	-27 18 28.0	0.0250	Sy2	8.32	0.51	23.03	O	4	<1.6	MCP
SWIFT J1238.6+0928	12 38 43.4	+09 27 37	0.08290	Sy2	0.58	0.92	23.52				
LEDA 170194	12 39 06.32	-16 10 47.8	0.0367	Sy2	3.77	2.00	22.46	O	3	<2.6	MCP
NGC 4593	12 39 39.43	-05 20 39.3	0.009	Sy1	7.12	3.72	20.30	O	5	<0.3	MCP

Table .1: continue

Name	RA	Dec	z	Class	F_{HX}^+	F_X^+	$\log N_H$	Notes	Rms*	L_{H2O}^{**}	Ref.***
IGR J12415-5750	12 41 25.74	-57 50 03.5	0.0242	Sy1.5	2.04	0.77	21.48	O	10 (1.3)	<16.1	K06
IGR J1248.2-5828	12 47 57.84	-58 30 00.2	0.028	Sy1.9	1.02	0.40	22.30				
NGC 4748	12 52 12.40	-13 24 53.0	0.0146	NLSy1	1.27	0.34	20.56	O	3	<0.4	MCP
ESO 323-32	12 53 20.19	-41 38 07.5	0.016	Sy2	1.81	0.40	25.00	O	13 (1.3)	<0.1	K06
3C 279	12 56 11.17	-05 47 21.5	0.5362	QSO/bl	2.15	0.60	20.35				
Mrk 783	13 02 58.84	+16 24 27.5	0.0672	NLSy1	2.21	0.65	21.18	O	2	<5.7	T11
IGR J13038+5348	13 03 59.43	+53 47 30.1	0.03	Sy1.2	2.74	1.59	20.22	O	4	<2.3	MCP
NGC 4941	13 04 13.08	-05 33 05.7	0.0037	Sy2	1.10	0.07	23.64	O	9	<0.1	MCP
IGR J13042-1020	13 04 14.38	-10 20 22.6	0.0104	Sy2	1.42	0.33	25.00	O	4	<0.3	MCP
NGC 4945	13 05 27.28	-49 28 04.4	0.0019	Sy2	25.60	0.54	24.72	M(D?,f)		205.5	B09
ESO 323-77	13 06 26.14	-40 24 52.2	0.015	Sy1.2	2.64	0.77	21.54	O	8	<1.1	MCP
IGR J13091+1137	13 09 05.65	+11 38 01.8	0.0291	XBONG	3.81	0.21	23.63	O	8	<4.3	this work
IGR J13107-5626	13 10 37.0	-56 26 55	-	AGN/RG	1.02	1.10	23.59				
IGR J13109-5552	13 10 43.35	-55 52 11.4	0.104	Sy1	2.43	0.49	<21.66				
IGR J13133-1109	13 13 05.8	-11 07 42	0.03427	Sy1	1.34	8.0	20.42	O	15 (1.3)	<48.3	K06
IGR J13149+4422	13 15 17.25	+44 24 25.9	0.0353	Sy2, L	2.15	0.75	22.72	O	4	<3.2	MCP
IGR J13168-7157	13 16 54.24	-71 55 27.0	0.0705	Sy1.5	1.08	0.38	21.21				
IGR J13187+0322	13 18 31.24	+03 19 48.9	0.606	QSO/bl?	>1.06	0.015	20.28				
NGC 5100	13 20 58.6	+08 58 55	0.03190	L	1.38	4.35	23.16				
MCG-03-34-063	13 22 19.06	-16 42 29.6	0.0213	Sy2	2.34	0.21	23.59	O	37 (0.66)	<23.4	B96
Cen A	13 25 27.61	-43 01 08.8	0.0018	Sy2	62.10	21.20	23.17	M(J?g)		1.0±0.1	O13
3C287.1	13 32 53.27	+02 00 45.7	0.2156	Sy1	<2.17	0.28	21.21				
ESO 383-18	13 33 26.30	-34 00 58.7	0.0124	Sy2	<0.76	0.52	23.29	O	14 (1.3)	<5.9	K06
MCG-06-30-015	13 35 53.80	-34 17 43.8	0.0077	Sy1.2	4.14	3.64	22.17	O	7	<0.3	this work
NGC 5252	13 38 16.00	+04 32 32.5	0.0230	Sy1.9	4.76	3.00	22.83	O	2	<0.7	MCP
IGR J13415+3033	13 41 11.17	+30 22 41.1	0.0398	Sy2	1.85	0.25	23.47	O	10	<10.0	MCP
SWIFT J1344.7+1934	13 44 15.6	+19 34 00	0.02706	Sy2/L	1.90	0.44	23.39	O	7	<3.2	MCP
IGR J13466+1921	13 46 28.46	+19 22 43.2	0.085	Sy1.2	2.07	0.32	20.27				
Cen B	13 46 49.04	-60 24 29.3	0.0129	RG/type2	1.13	0.49	22.11				
4U 1344-60	13 47 36.00	-60 37 03.8	0.013	Sy1.5	7.23	3.57	23.67				
IGR J13477-4210	13 48 15.2	-42 10 20	0.03860	Sy2	<0.83	1.19	22.80				
IC 4329A	13 49 19.29	-30 18 34.4	0.0160	Sy1.2	20.90	10.40	21.54	O	28	<4.5	this work
1AXG J135417-3746	13 54 16.10	-37 46 43.0	0.0509	Sy1.9	1.42	0.34	22.80				
IGR J13550-7218	13 55 11.45	-72 18 51.3	0.071	Sy2	1.49	0.22	23.28				
PKS 1355-416	13 59 00.2	-41 52 53	0.31300	Sy1	0.75	1.16	21.43				
IGR J14080-3023	14 08 06.57	-30 23 52.6	0.0237	Sy1.5	1.89	0.64	20.56	O	25 (1.3)	<38.5	K06
SWIFT J1410.9-4229	14 10 44.8	-42 28 33	0.03394	Sy2	1.02	2.07	22.76				
Circinus Galaxy	14 13 08.90	-65 20 27.0	0.0014	Sy2	20.20	1.00	24.60	M(D+O,h)		44.9	B09
NGC 5506	14 13 14.87	-03 12 27.0	0.0062	Sy2	14.90	8.38	22.53	M(J/O,e)		28±11	T11
IGR J14175-4641	14 17 03.94	-46 41 39.1	0.076	Sy2	1.62	0.095	23.88				
SWIFT J1417.7+2539	14 17 56.7	+25 43 26	0.23700	BL Lac	2.17	12.0	20.19				
NGC 5548	14 17 59.51	+25 08 12.5	0.0172	Sy1.5	3.00	5.30	20.19	O	5	<0.9	MCP
ESO 511-G030	14 19 22.44	-26 38 40.8	0.0224	Sy1	3.42	1.30	20.70				
H 1419+480	14 21 29.25	+47 47 21.4	0.0723	Sy1.5	<1.76	0.70	20.83				

Table .1: continue

Name	RA	Dec	z	Class	F_{HX}^+	F_X^+	$\log N_H$	Notes	Rms*	$L_{H_2O}^{**}$	Ref.***
H 1426+428	14 28 32.57	+42 40 24.8	0.1291	BL Lac	1.79	3.38	21.01				
IGR J14301-4158	14 30 12.17	-41 58 31.4	0.0039	Sy2	0.92	0.27	22.08				
NGC 5643	14 32 40.70	-44 10 28.0	0.0040	Sy2	1.10	0.084	23.85	M(?)		13±5	MCP
NGC 5674	14 33 52.2	+05 27 30	0.02493	Sy1.9	1.81	4.85	23.05	O	4	<1.6	MCP
SWIFT J1436.8-1615	14 36 49.6	-16 13 41	0.14454	Sy1/QSO	2.00	7.19	20.88				
NGC 5728	14 42 23.90	-17 15 11.0	0.0093	Sy2	5.38	0.15	24.14	M(D,c)		100±15	MCP
IGR J14471-6414	14 46 28.26	-64 16 24.3	0.053	Sy1.2	1.11	0.48	21.60				
IGR J14471-6319	14 47 14.88	-63 17 19.2	0.038	Sy2	1.36	0.39	22.39				
IGR J14488-4008	14 48 51.0	-40 08 46	0.12300	Sy1.2	0.75	5.27	22.89				
IGR J14492-5535	14 49 17.3	-55 35 45	-	AGN	1.81	3.10	23.08				
IGR J14515-5542	14 51 33.13	-55 40 38.4	0.018	Sy2	2.08	0.53	21.52				
PKS 1451-375	14 54 27.4	-37 47 33	0.31405	Sy1.2	0.98	3.18	20.80				
IGR J14552-5133	14 55 17.80	-51 34 17.0	0.016	NLSy1	1.45	0.96	21.53				
IGR J14561-3738	14 56 08.43	-37 38 52.4	0.024	Sy2	1.55	0.002	>24				
IC 4518A	14 57 41.16	-43 07 55.2	0.0163	Sy2	2.08	0.29	23.15	O	9	<1.5	this work
IRXS J150101.7+223812	15 01 01.8	+22 38 06	0.23500	BL Lac	3.69	0.70	20.54				
MKN 841	15 04 01.20	+10 26 16.1	0.0364	Sy1.5	<3.40	1.62	20.84	O	4	<3.4	MCP
SWIFT J1508.6-4953	15 08 39.0	-49 53 02	-	bl	0.96	2.80	21.31				
IRAS 15091-2107	15 11 59.80	-21 19 02.0	0.0446	NLSy1	2.44	0.90	21.15	O	2	<3.0	T11
PKS 1510-089	15 12 50.5	-09 06 00	0.36000	QSO/bl	3.85	6.31	20.84				
SWIFT J1513.8-8125	15 14 41.92	-81 23 38.9	0.06836	Sy1.2	1.83	1.11	21.88				
ESO 328-36	15 14 47.2	-40 21 35	0.02370	Sy1.8	0.85	7.13	20.84	O	11 (1.3)	<16.9	K06
IGR J15161-3827	15 15 59.70	-38 25 46.8	0.0365	Sy2	<6.22	0.12	22.00				
IGR J15301-3840	15 30 08.0	-38 39 07	0.01553	Sy2	0.77	3.34	22.36				
IGR J15311-3737	15 30 51.79	-37 34 57.3	0.127	Sy1	0.89	1.86	21.32				
MCG-01-40-001	15 33 20.7	-08 42 02	0.02271	Sy2	1.77	4.27	22.59	O	13 (1.3)	<18.4	K06
IGR J15359-5750	15 36 02.8	-57 48 53	-	AGN	2.06	4.97	23.30				
IGR J15415-5029	15 41 26.4	-50 28 23	0.03200	Sy2?	1.04	0.54	<22.04				
NGC 5995	15 48 24.95	-13 45 28.0	0.0252	Sy1.9	3.47	2.20	21.93	O	5	<2.0	MCP
IGR J15539-6142	15 53 35.28	-61 40 58.4	0.015	Sy2	1.58	0.073	23.24				
IGR J15549-3740	15 54 46.76	-37 38 19.1	0.019	Sy2	1.72	0.34	22.76				
IGR J16024-6107	16 01 48.23	-61 08 54.7	0.011	Sy2	0.92	0.30	21.40				
IGR J16056-6110	16 05 51.17	-61 11 44.0	0.052	Sy1.5	1.30	0.14	21.31				
IGR J16058-7253 (1)	16 06 06.9	-72 52 42	0.09000	Sy2	0.90	3.18	23.58				
IGR J16058-7253 (2)	16 05 23.2	-72 53 56	0.06900	Sy2?	0.60	3.50	23.24				
IGR J16119-6036	16 11 51.36	-60 37 53.1	0.016	Sy1.5	2.53	0.33	21.36				
IGR J16185-5928	16 18 36.44	-59 27 17.4	0.035	NLSy1	1.55	0.27	23.02				
Mrk 1498	16 28 04.0	+51 46 31	0.05470	Sy1.9	5.09	9.00	23.76				
SWIFT J1630.5+3925	16 30 32.6	+39 23 03	0.03056	Sy2	1.59	1.25	23.60	M(J/O?,i)		20±10	MCP
IGR J16351-5806	16 35 13.17	-58 04 49.7	0.0091	Sy2	1.96	0.031	24.68	O	13 (1.3)	<3.0	K06
IGR J16385-2057	16 38 30.91	-20 55 24.6	0.0269	NLSy1	1.27	0.53	21.08	M(J/O?,f)		12±2	this work****
IGR J16426+6536	16 43 04.07	+65 32 50.9	0.323	NLSy1	3.45	0.0085	20.41				
IGR J16482-3036	16 48 15.20	-30 35 03.7	0.0313	Sy1	<3.85	2.00	21.00	O	34	<21.1	this work
SWIFT J1650.5+0434	16 50 42.70	+04 36 18.0	0.0321	Sy2	2.19	0.32	22.68				

Table .1: continue

Name	RA	Dec	z	Class	$F_{H\alpha}^+$	F_X^+	Log N_H	Notes	Rms*	L_{H2O}^{**}	Ref.***
NGC 6221	16 52 46.32	-59 13 00.8	0.005	Sy2	1.06	1.41	22.04	O	11 (1.3)	<0.8	K06
ESO 138-1	16 51 20.21	-59 14 04.2	0.0091	Sy2	1.06	0.180	24.18	O	13 (1.3)	<3.0	K06
NGC 6240	16 52 58.97	+02 24 01.7	0.0245	Sy2/L	5.42	0.20	24.30	M(D ² ,j)		40±20	MCP
Mrk 501	16 53 52.22	+39 45 36.6	0.0337	BL Lac	4.32	16.7	20.07	O	4	<2.9	MCP
IGR J16558-5203	16 56 05.62	-52 03 40.9	0.054	Sy1.2	2.89	1.75	23.27				
SWIFT J1656.3-3302	16 56 16.85	-33 02 11.1	2.4	QSO/bl	3.04	0.44	21.34				
IGR J17009+3559	17 00 53.00	+35 59 56.2	0.113	XBONG	2.13	0.11	23.7				
IGR J17036+3734	17 03 20.20	+37 37 24.9	0.065	Sy1	2.01	0.21	20.39				
IGR J17111+3910	17 11 05.3	+39 08 49	-	AGN	0.96	1.47	20.55				
NGC 6300	17 16 59.47	-62 49 14.0	0.0037	Sy2	6.51	0.86	23.38	M(?)		3.5	B09
MCG+08-31-041	17 19 14.45	+48 58 49.6	0.0242	Sy1/L	7.66	1.10	21.22	O	4	<1.5	MCP
IGR J17204-3554	17 20 21.6	-35 54 32	-	AGN	1.15	2.50	23.20				
Mrk 506	17 22 39.9	+30 52 53	0.04303	Sy1.5	1.81	6.30	<20.70	O	3	<3.5	MCP
SWIFT J1723.5+3630	17 23 23.2	+36 30 10	0.04000	Sy1.5	1.79	8.39	21.28	O	4	<4.0	MCP
PKS 1730-13	17 33 02.7	-13 04 50	0.90200	QSO/bl	1.30	1.46	21.94				
IGR J17348-2045	17 34 59.1	-20 45 34	0.044	Sy2	1.7	2.2	23.23				
GRS 1734-294	17 37 28.35	-29 08 02.5	0.0214	Sy1	8.25	3.84	21.32	O	8	<2.3	this work
IGR J17379-5957	17 37 39.1	-59 56 27	0.01702	Sy2	1.17	6.02	20.79	O	17 (1.3)	<13.5	K06
2E 1739.1-1210	17 41 55.25	-12 11 56.6	0.037	Sy1.2	2.89	1.29	21.18	O	10	<8.7	this work
PKS 1741-03	17 43 58.8	-03 50 05	1.05400	QSO/bl	0.70	2.09	21.27				
IGR J17448-3232	17 44 55.0	-32 32 00	0.05500	Cluster/bl	1.11	1.65	22.40				
IGR J17488-2338	17 48 39.0	-23 35 21	0.24000	Sy1.5	1.58	2.0	22.06				
IGR J17476-2253	17 47 29.71	-22 52 44.3	0.0463	Sy1	1.81	0.26	21.48				
IGR J17488-3253	17 48 55.13	-32 54 52.1	0.02	Sy1	3.96	1.40	21.53	O	9	<2.3	this work
IGR J17513-2011	17 51 13.62	-20 12 14.6	0.047	Sy1.9	2.43	0.58	21.82	O	12	<16.8	this work
IGR J17520-6018	17 51 55.8	-60 19 43	0.11200	Sy2	2.19	2.55	23.11				
IRXS J17525.0-053210	17 52 52.00	-05 32 10.0	0.136	Sy1.2	1.00	0.26	21.33				
NGC 6552	18 00 07.2	+66 36 54	0.02649	Sy2	0.85	0.43	23.85	O	13 (1.3)	<25.0	K06
IGR J18027-1455	18 02 47.37	-14 54 54.8	0.035	Sy1	3.85	0.66	21.48	O	5	<3.9	this work
IGR J18078+1123	18 07 49.9	+11 20 49	0.07800	Sy1.2	1.26	6.32	22.25				
IGR J18129-0649	18 12 50.9	-06 48 24	0.77500	Sy1/QSO	0.66	2.74	21.54				
SWIFT J1821.6+5953	18 21 26.8	+59 55 21	0.0990	Sy2	1.41	1.49	22.88				
IGR J18218+6421	18 21 57.24	+64 20 36.2	0.297	Sy1.2	1.73	1.24	20.54				
IGR J18244-5622	18 24 19.39	-56 22 09.1	0.0169	Sy2	2.66	0.67	23.15				
IGR J18249-3243	18 24 55.92	-32 42 57.7	0.355	Sy1/QSO	1.02	0.52	21.14				
IGR J18259-0706	18 25 57.58	-07 10 22.8	0.037	Sy1	1.36	0.54	21.91	O	5	<4.3	this work
IGR J18308+0928	18 30 50.6	+09 28 42	0.01900	Sy2	1.32	1.30	23.08				
IGR J18311-3337	18 31 14.75	-33 36 08.5	0.0687	Sy2	1.66	0.026	22.15				
PKS 1830-211	18 33 39.92	-21 03 39.9	2.507	QSO/bl	4.83	1.00	22.00				
3C382	18 35 03.39	+32 41 46.8	0.0579	Sy1	5.91	5.98	20.79	O	3	<6.4	MCP
Fairall 49	18 36 58.3	-59 24 09	0.02002	Sy2	1.51	12.0	22.09	O	11 (1.3)	<12.1	K06
ESO 103-35	18 38 20.30	-65 25 41.0	0.0133	Sy2	8.15	2.40	23.27	M(?)		460.5	B09
3C 390.3	18 42 08.99	+79 46 17.1	0.0561	Sy1.5	6.13	2.14	20.63	O	4	<8.0	this work
ESO 140-43	18 44 54.01	-62 21 53.2	0.0142	Sy1.5	3.93	9.50	23.04	O	72 (0.84)	<25.7	B96

Table .1: continue

Name	RA	Dec	z	Class	$F_{H\alpha}^+$	F_X^+	$\log N_H$	Notes	Rms*	L_{H2O}^{**}	Ref.***
SWIFT J1845.4+7211	18 45 26.2	+72 11 02	0.04630	Sy2	1.00	4.22	22.51	O	2	<2.7	MCP
IGR J18470-7831	18 47 02.83	-78 31 49.5	0.0743	Sy1	1.83	0.80	20.08	O	50 (0.84)	<489.1	G02
PBC J1850.7-1658	18 50 51.6	-16 55 58	-	AGN/RG	1.28	2.19	22.17				
IGR J18538-0102	18 53 48.4	-01 02 30	0.14500	Sy1	1.02	4.0	21.61	O	16 (1.3)	<37.4	K06
ESO 25-2	18 54 40.39	-78 53 54.4	0.0292	Sy1	2.15	0.20	20.92	O	3	<13.4	this work
2E 1853.7+1534	18 56 00.00	+15 38 13.0	0.084	Sy1	2.36	1.22	21.59	O	20 (1.3)	<96.7	K06
2E 1849.2-7832	18 57 07.68	-78 28 21.3	0.0420	Sy1	3.27	0.77	20.92	O			
IGR J19077-3925	19 07 50.36	-39 23 31.9	0.076	Sy1.9	1.49	0.36	21.15				
IGR J19118-1707	19 11 42.64	-17 10 05.1	0.0234	L	<1.17	0.14	23.02				
PKS 1916-300	19 19 28.01	-29 58 09.7	0.1668	Sy1.5-1.8	<1.23	0.62	20.90				
ESO 141-G055	19 21 14.13	-58 40 13.3	0.0371	Sy1.2	4.65	2.45	20.68				
IRXS J192450.8-291437	19 24 51.06	-29 14 30.1	0.352	BL Lac	1.43	0.81	20.86				
SWIFT J1930.5+3414	19 30 13.81	+34 10 49.8	0.0629	Sy1.5-1.8	1.73	0.22	23.44				
SWIFT J1933.9+3258	19 33 47.1	+32 54 26	0.0565	Sy1.2	1.30	13.8	<20.6				
QSO B1933-400	19 37 16.22	-39 58 01.5	0.9655	QSO/bl	1.32	0.19	21.11		5	<0.4	this work
IGR J19378-0617	19 37 33.00	-06 13 05.0	0.0106	NLSy1	1.83	2.70	23.50		8	<0.1	MCP
IGR J19405-3016	19 40 15.07	-30 15 52.2	0.052	Sy1.2	<1.47	0.11	20.96		4	<7.4	MCP
NGC 6814	19 42 40.40	-10 19 24.0	0.0052	Sy1.5	5.66	0.17	21.10				
IGR J19443+2117	19 43 56.2	+21 18 23	-	BL Lac?	1.00	18.3	21.73				
XSS J19459+4508	19 47 32.88	+44 52 58.8	0.0539	Sy2	1.98	0.41	23.04				
IGR J19491-1035	19 49 08.69	-10 34 34.5	0.0246	Sy1.2	1.33	0.56	22.26				
3C 403	19 52 15.82	+02 30 24.3	0.059	Sy2	2.02	1.30	23.60	M(J,a)	6	1426±174	T03
Cyg A	19 59 28.36	+40 44 02.1	0.0561	Sy2	8.34	1.20	23.30	O		<11.9	MCP
IES 1959+650	19 59 59.8	+65 08 55	0.04700	BL Lac	1.57	91.7	20.85				
ESO 399-20	20 06 57.95	-34 32 54.6	0.0249	NLSy1	1.75	0.13	20.85				
NGC 6860	20 08 46.90	-61 06 01.0	0.01488	Sy1.5	3.90	1.80	21.00		78 (0.84)	<30.6	B96
IGR J20159+3713	20 15 28.8	+37 11 00	0.857	QSO/bl	1.11	2-5 (var)	21.89				
SWIFT J2018.4-5539	20 18 01.3	-55 39 31	0.06063	Sy2	3.64	4.01	23.50				
IGR J20186+4043	20 18 38.71	+40 41 00.3	0.0144	Sy2	2.30	0.28	22.76	O	4	<0.5	this work
IGR J20216+4359	20 21 49.04	+44 00 39.4	0.017	Sy2	1.32	0.56	23.11				
IGR J20286+2544(1)	20 28 35.10	+25 43 59.5	0.0139	Sy2/SB	3.34	2.11	23.78	O	4	<0.5	MCP
IGR J20286+2544(2)	20 28 28.90	+25 43 24.6	0.0144	XBONG	1.28	<1.6	23.97	O	33 (1.6)	<23.1	H84
NGC 6926	20 33 06.1	-02 01 39	0.01961	Sy2	1.36	0.07	24.00	M(D?,k)		410±80	MCP
4C +21.55	20 33 32.0	+21 46 22	0.17350	Sy1	2.91	14.0	21.78				
4C 74.26	20 42 37.18	+75 08 02.5	0.104	Sy1	4.27	2.53	21.15	O	4	<27.4	this work
SWIFT J2044.0+2832	20 44 04.00	+28 33 03.0	0.05	Sy1	2.62	0.71	21.24				
Mrk 509	20 44 09.77	-10 43 24.4	0.0344	Sy1.5	7.63	3.4	20.63	O	3	<2.2	MCP
IGR J20450+7530	20 44 34.49	+75 31 58.9	0.095	Sy1	<3.57	0.032	20.30				
S52116+81	21 14 00.00	+82 04 47.0	0.084	Sy1	<2.76	1.21	21.38	O	3	<13.4	this work
IGR J21178+5139	21 17 47.2	+51 38 54	-	AGN	1.81	2.1	22.32				
IRXS J211928.4+333259	21 19 29.13	+33 32 57.0	0.051	Sy1.5	1.55	0.59	21.52				
IGR J21247+5058	21 24 39.33	+50 58 26.0	0.020	Sy1	12.60	4.88	22.89	O	19	<4.8	this work
SWIFT J2127.4+5654	21 27 45.58	+56 56 35.6	0.0147	NLSy1	3.14	4.2	21.90	O	3	<0.4	MCP
CTS 109	21 32 02.1	-33 42 54	0.02997	Sy1.2	1.98	7.6	20.55				

Table .1: continue

Name	RA	Dec	z	Class	F_{JX}^*	F_X^*	$\log N_H$	Notes	Rms*	L_{420}^{**}	Ref.***
RX J2135.9+4728	21 35 54.2	+47 28 22.3	0.025	Sy1	1.79	0.62	20.30	O	3	<1.2	this work
IRXS J213944.3+595016	21 39 45.10	+59 50 14.0	0.114	Sy1.5	1.02	0.59	21.54				
PKS 2149-306	21 51 55.52	-30 27 53.7	2.345	QSO/bl	2.51	0.80	20.34				
IGR J21565+5948	21 56 04.20	+59 56 04.5	0.208	Sy1	0.98	0.12	21.81				
SWIFT J2156.2+1724	21 56 15.2	+17 22 53	0.03400	Sy1.8	2.00	1.77	23.33				
Mrk 520	22 00 41.37	+10 33 08.7	0.0266	Sy1.9	4.13	0.63	22.38	O	2	<0.9	MCP
NGC 7172	22 02 01.90	-31 52 11.6	0.0087	Sy2	7.93	4.30	22.86	O	7	<0.3	MCP
BL Lac	22 02 43.29	+42 16 40.0	0.686	BL Lac	2.40	2.02	21.44	O	8	<2382.3	this work
UGR 12040	22 27 05.8	+36 21 42	0.02133	Sy1.9	2.62	0.86	<22.9	O	5	<1.4	MCP
IGR J22292+6647	22 29 13.84	+66 46 51.5	0.112	Sy1.5	1.11	0.69	21.68				
NGC 7314	22 35 46.23	-26 03 00.9	0.0048	Sy1.9	3.02	1.91	22.02	O	5	<0.1	MCP
IGR J22367-1231	22 36 46.49	-12 32 42.6	0.0241	Sy1.9	2.76	1.09	23.35	O	4	<1.5	MCP
3C 452	22 45 49.10	+39 41 15.0	0.0811	Sy2	3.00	0.50	23.77	O	2	<8.3	MCP
IGR J22517+2218	22 51 53.50	+22 17 37.3	3.668	QSO/bl	3.15	0.26	22.48				
3C 454.3	22 53 57.75	+16 08 53.6	0.859	QSO/bl	19.17	6.10	21.28	O	4	<10.4	this work
QSO B2251-178	22 54 05.88	-17 34 55.3	0.0640	Sy1.2	6.66	2.00	22.33				
KAZ 320	22 59 32.9	+24 55 06	0.03450	NLSy1	1.49	10.1	20.68				
NGC 7465	23 02 00.95	+15 57 53.6	0.0066	Sy2/L	2.62	0.41	23.66	O	3	<0.1	MCP
NGC 7469	23 03 15.75	+08 52 25.9	0.0163	Sy1.5	4.49	2.30	20.46	O	6	<1.0	MCP
MCG-02-58-022	23 04 43.48	-08 41 08.6	0.0469	Sy1.5	4.30	3.18	20.56	O	3	<4.2	this work
NGC 7479	23 04 56.6	+12 19 22	0.00794	Sy1.9	1.40	0.33	24.30	M(D?,1)		12±8	MCP
NGC 7582	23 18 23.49	-42 22 14.1	0.0052	Sy2	<2.80	0.23	24.04	O	10	<0.2	MCP
IGR J23206+6431	23 20 36.58	+64 30 45.2	0.0717	Sy1	<0.66	0.55	21.95				
RHS 61	23 25 54.2	+21 53 14	0.12000	Sy1	1.43	4.32	20.59				
PKS 2325+093	23 27 33.6	+09 40 09	1.84300	QSO/bl	2.45	2.9	20.60				
IGR J23308+7120	23 30 37.68	+71 22 46.6	0.037	Sy2?	<0.53	0.14	22.96	O	2	<1.7	this work
IGR J23524+5842	23 52 22.11	+58 45 30.7	0.164	Sy2?	1.23	0.28	22.46	O	3	<51.1	this work
IGR J23558-1047	23 55 59.3	-10 46 45	1.10800	Sy1/QSO	5.26	0.08					

Sources in boldface belong to the complete AGN catalog reported in Malizia et al. (2009). The format on the relevant digits in the coordinates are those originally reported Malizia et al. (2012, 2016). Maser types: D=disc; J=jet; O=outflow; /=or; +=plus. For possible limits on this classification see Sect. 6. References for the Maser type: a) MCP at <https://safe.nrao.edu/wiki/bin/view/Main/PublicWaterMaserList> (web page updated at November 10, 2018); b) Henkel et al. (2005); c) Kamali et al. (2017); d) Kondratko et al. (2005); e) Tarchi et al. (2011b); f) Humphreys et al. (2016); g) Ott et al. (2013); h) Greenhill et al. (2003b); i) Greenhill et al. (2009); j) Hagiwara & Edwards (2015); k) Sato et al. (2005); l) Wang et al. (2010). † 2–10 keV and 20–100 keV flux in units of 10^{-11} erg cm^{-2} s^{-1} * 1σ rms in mJy, calculated over a 0.3 km s^{-1} wide channel, unless otherwise specified (different channel widths are reported in brackets); ** Water maser isotropic luminosities are in unit of L_\odot , where $L_\odot = 3.826 \times 10^{33} \text{ erg s}^{-1}$. We calculate the upper limits for the undetected sources using the formula: $L_{420}[L_\odot] = 0.023 \times S[\text{Jy}] \times \Delta v[\text{km s}^{-1}] \times D^2[\text{Mpc}^2]$, where $S[\text{Jy}]$ and $\Delta v[\text{km s}^{-1}]$, are the 5σ rms and the channel spacing, respectively; D is the distance in Mpc, derived using the redshift in column 4 and $H_0 = 70 \text{ km s}^{-1} \text{ Mpc}^{-1}$ *** References for the rms (undetected sources) or the isotropic maser luminosity (detected sources): B96: Braatz et al. (1996); B09: Bennert et al. (2009) and references therein; G96: Gallimore et al. (1996); G02: Greenhill et al. (2002); H84: Henkel et al. (1984); K05: Kamenno et al. (2005); K06: Kondratko et al. (2006a); MCP: Megamaser Cosmology Project webpage (<https://safe.nrao.edu/wiki/bin/view/Main/MegamaserCosmologyProject>); O13: Ott et al. (2013); P03: Peck et al. (2003); P15: Pesce et al. (2015); T03: Tarchi et al. (2003); T11: Tarchi et al. (2011b). **** The maser in IGRJ16385-2057 was detected during our survey (Sect. 3.3), a detailed analysis have been reported in Tarchi et al. (2011b).

Appendix A: Tables with the total sample, detection fractions in Swift/BAT and Diamond-Stanic samples

Table 1A lists all 380 INTEGRAL/IBIS AGN with their optical coordinates, redshift, class, hard X-ray (20–100 keV) flux, X-ray (2–10 keV) flux, X-ray column density, a note to indicate if the source was observed or not at 22 GHz, which maser type was detected and relative references. Finally, for those sources for which maser emission was detected, we also list the reported water maser isotropic luminosity and the reference to the maser data; for objects observed at 22 GHz but not detected, the 1σ rms and an upper limit to the maser luminosity are reported. Objects belonging to the complete sample are highlighted in boldface in Table 1A for clarity.

In Table 2A we report the 17 detected sources from the Swift/BAT 9 catalogue with their names, optical classification as type 1 or 2 AGN and coordinates. Analogously, in Table 3A, the 21 AGN detected at 22 GHz from the Diamond-Stanic et al. (2009) sample have been reported.

Appendix B: Maser Types

Among INTEGRAL AGN with maser detection, only 6 sources (IGR J05081+1722, NGC 3081, NGC 3783, NGC 5643, NGC 6300 and ESO 103-G35) have no associated maser type yet. Here we discuss each source individually providing some clues on their most likely maser type.

IGR J05081+1722 is interesting from many points of view. It belongs to an infrared-luminous interacting pair of galaxies, characterized by a luminosity for the whole system (made of a combination of star formation and accretion) of $\log(L_{IR}/L_{\odot})=11.2$. The system is at an early-stage of merger (11.3 kpc distance) and is known to host an AGN optically classified as Seyfert 2 plus a normal galaxy. The AGN which is also the component in the system that displays water maser emission hosts molecular outflow and probably also a disc wind (Yamashita et al. 2017, Ballo et al. 2015). NGC 3783 is one of the most intensively monitored Seyfert galaxy at high energies. It is known to exhibit UV absorbers plus a series of ionized X-ray absorbers, variable in time (Fukumara et al. 2018, Mehdipour et al. 2017), generally interpreted as associated to a strong obscuring outflow in the nuclear region. Contrary to other sources in our sample, both IGR J05081+1722 and NGC 3783 do not display strong X-ray absorption (the column density in both is around 10^{22} at cm^{-2}) suggesting that their water maser emission could indeed be associated to jet or outflow. Since no clear jet emission seems to be present in NGC 3783, but only a diffuse radio emission on tens of pc-scales (Orienti & Prieto 2010), the outflow remains the only option; in IGR J05081+1722 the situation is less clear but the outflow is a viable possibility to explain water maser emission also in this source.

Indeed, single-dish maser spectra for these sources¹¹, are consistent with an outflow origin. In particular, the maser emission in IGR J05081+1722 is blueshifted with respect to the systemic velocity (by ~ 100 km/s) and appears to consist of a handful of narrow components sitting on a broader feature. The maser spectrum in NGC 3783 is instead characterized by a group of narrow features, close to the systemic velocity of the galaxy. Clearly, without high-resolution follow-up studies, the nature of the maser cannot be uniquely assessed.

¹¹ As shown in the MCP webpage

NGC 6300 and ESO 103-G35 are type 2 mildly absorbed AGN with column density around 10^{23} at cm^{-2} . NGC 6300 features a slightly resolved radio core at arcsecond resolution with extension in the southern direction (Morganti et al. 1999) plus evidence for a complex molecular hydrogen structure made of an edge-on outflow superimposed on a rotating disc (Davies et al. 2014). ESO 103-G35 does not show evidence for a radio jet; furthermore an in depth analysis of the galaxy optical properties brought no clues on the origin of water maser emission including no evidence for outflows (Bennert et al. 2004). Despite this, the source has been reported in X-rays as the site of a highly ionized outflow (Gofford et al. 2015). As in the two previous cases, the interpretation (among others) of an outflow origin of the water maser emission does not conflict with the shape of the maser spectra¹² for both NGC 6300 (Greenhill et al. 2003b) and ESO 103-G35. In both cases, emission is detected close to (or slightly redshifted w.r.t.) the systemic velocity of the target, and is comprised of a very small number of narrow features (one in the case of ESO 103-G35) placed above a broader component¹³.

Finally NGC 5643 and NGC 3081 are heavily absorbed objects (with NGC 3081 being also Compton thick). In these objects nuclear discs are likely to be the site where maser emission develops. Indeed recent observations with ALMA of NGC 5643 (Alonso-Herrero et al. 2018) have resolved at the parsec scale a massive rotating disc/torus of molecular gas with strong non nuclear motion features associated to radial outflow in the disc. Interestingly the maser emission seems to be centrally located with respect to the inner (nuclear) part of this structure, which is also tilted with respect to the larger scale disc. The inner structure of NGC 3081 has instead been mapped with the Gemini Multi Object Spectrograph (GMOS-IFU) (Schnorr-Müller et al. 2016) and found to host an even more complex structure albeit at the kilo parsec scale: this includes rotation in the galaxy disc plane, a bipolar outflow from the AGN, non-circular motions along the nuclear bar, and an interaction between the bipolar outflow and the disc gas. Both objects thus resemble the well known maser sources NGC 1068 and Circinus galaxy where water maser disc emission is coupled to jet/outflow maser radiation thus suggesting a similar interpretation also for NGC 5643 and NGC 3081. From the single-dish spectrum alone¹⁴, due to its relatively low signal-to-noise ratio, it is not possible to infer a secure hypothesis on the nature of the maser in NGC 3081. The maser in NGC 5643 (Greenhill et al. 2003b, and MCP webpage) indicates, instead, a redshifted (50–100 km/s with respect to the systemic velocity) emission, constituted by a relatively broad feature with two or three peaks, possibly due to a blending of features. Speculatively, the maser could then be either associated to a jet (a diffuse radio jet on both side of the nucleus is indeed visible in a high sensitivity VLA image (Leipski et al. 2006)) or to a rotating structure of which we are only seeing the redshifted lines or the systemic ones, when accounting for a large uncertainty in the reported target recessional velocity.

As mentioned before, however, confident clues on the association of the maser emission with the AGN activity and on the maser nature of all six objects must await follow-up (interferometric) studies. In particular, all these maser sources, with the exception of ESO 103-G35 (~ 460 solar luminosities), have moderate maser isotropic luminosities: four targets have

¹² As shown in the MCP webpage

¹³ A somewhat different spectrum of ESO 103-G35 is, however, shown in the detection paper (Braatz et al. 1996), where emission form a single, 20-km/s wide line is shown, clearly redshifted by ~ 100 km/s with respect to the systemic velocity.

¹⁴ Shown in the MCP webpage

Table 2A: AGN in the BAT 9 month survey sample with water maser detections

Name (class)	RA(J2000), Dec(J2000)	Name (class)	RA(J2000), Dec(J2000)
NGC235A(2)	00 42 52.81, -23 32 27.7	NGC4945(2)	13 05 27.28, -49 28 04.4
Mkn348(2)	00 48 47.10, +31 57 25.0	NGC5128(2)	13 25 27.61, -43 01 08.8
MKN3(2)	06 15 36.31, +71 02 14.9	NGC5506(2)	14 13 14.87, -03 12 27.0
NGC3081(2)	09 59 29.54, -22 49 34.6	NGC5728(2)	14 42 23.90, -17 15 11.0
NGC3783(1)	11 39 01.78, -37 44 01.7	NGC6240(2)	16 52 58.97, +02 24 01.7
NGC4051(1)	12 03 09.62, +44 31 52.8	NGC6300(2)	17 16 59.47, -62 49 14.0
NGC4151(1)	12 10 32.66, +39 24 20.7	ESO103-G35(2)	18 38 20.30, -65 25 41.0
Mrk766(1)	12 18 26.48, +29 18 14.0	3C403(2)	19 52 15.82, +02 30 24.3
NGC4388(2)	12 25 46.93, +12 39 43.3		

Table 3A: Maser Galaxies in the Diamond-Stanic et al. (2009) sample

Name (class)	RA(J2000), Dec(J2000)	Name(class)	RA(J2000), Dec(J2000)
NGC1068(2)	02 42 40.70, -00 00 48.0	NGC4258(2)	12 18 57.62, +47 18 14.0
NGC1386(2)	03 36 46.24, -35 59 57.0	NGC4388(2)	12 25 46.93, +12 39 43.3
NGC2273(2)	06 50 08.67, +60 50 44.8	NGC4945(2)	13 05 27.28, -49 28 04.4
NGC2639(2)	08 43 38.09, +50 12 19.9	NGC5128(2)	13 25 27.61, -43 01 08.8
NGC3081(2)	09 59 29.54, -22 49 34.6	Circinus(2)	14 13 08.90, -65 20 27.0
NGC3079(2)	10 01 57.80, +55 40 47.2	NGC5506(2)	14 13 14.87, -03 12 27.0
IC2560(2)	10 16 18.71, -33 33 49.7	NGC5643(2)	14 32 40.70, -44 10 28.0
NGC3735(2)	11 35 57.33, +70 32 08.1	NGC5728(2)	14 42 23.90, -17 15 11.0
NGC3783(1)	11 39 01.78, -37 44 01.7	NGC6300(2)	17 16 59.47, -62 49 14.0
NGC4051(1)	12 03 09.62, +44 31 52.8	NGC7479(2)	23 04 56.67, +12 19 22.4
NGC4151(1)	12 10 32.66, +39 24 20.7		

luminosities only slightly above the paradigmatic threshold that separate kilo and megamasers (35, 20, 17, and 13 solar luminosities for IGR J05081+1722, NGC 3783, NGC 3081, and NGC 5643, respectively), and one objects, NGC 6300 (~ 3.5 solar luminosities) is below that threshold. While this is still consistent with an outflow-related origin of the maser emission (Tarchi et al. 2011a, discuss an analogous origin for the water maser detected in a sample of NLSy1 that, indeed, have similar luminosities to the present ones), an association with star formation activity for these masers, especially for that in NGC 6300, cannot be a priori ruled out.